AFRL-AFOSR-VA-TR-2018-0282

2D (Two Dimensional) Heterostructures for Integrated Nano-Optoelectronics

Xiaodong Xu
UNIVERSITY OF WASHINGTON

12/11/2017
Final Report

Air Force Research Laboratory
AF Office Of Scientific Research (AFOSR)/ RTB1
Arlington, Virginia 22203
Air Force Materiel Command

DISTRIBUTION A: Distribution approved for public release.

REPORT DOCUMENTATION PAGE

Form Approved
OMB No. 0704-0188

1. REPORT DATE *(DD-MM-YYYY)*	2. REPORT TYPE	3. DATES COVERED *(From - To)*
27-07-2018	Final Performance	15 Sep 2014 to 14 Sep 2017

4. TITLE AND SUBTITLE
2D (Two Dimensional) Heterostructures for Integrated Nano-Optoelectronics

5a. CONTRACT NUMBER

5b. GRANT NUMBER
FA9550-14-1-0277

5c. PROGRAM ELEMENT NUMBER
61102F

6. AUTHOR(S)
Xiaodong Xu

5d. PROJECT NUMBER

5e. TASK NUMBER

5f. WORK UNIT NUMBER

7. PERFORMING ORGANIZATION NAME(S) AND ADDRESS(ES)
UNIVERSITY OF WASHINGTON
4333 BROOKLYN AVE NE
SEATTLE, WA 98195-0001 US

8. PERFORMING ORGANIZATION REPORT NUMBER

9. SPONSORING/MONITORING AGENCY NAME(S) AND ADDRESS(ES)
AF Office of Scientific Research
875 N. Randolph St. Room 3112
Arlington, VA 22203

10. SPONSOR/MONITOR'S ACRONYM(S)
AFRL/AFOSR RTB1

11. SPONSOR/MONITOR'S REPORT NUMBER(S)
AFRL-AFOSR-VA-TR-2018-0282

12. DISTRIBUTION/AVAILABILITY STATEMENT
A DISTRIBUTION UNLIMITED: PB Public Release

13. SUPPLEMENTARY NOTES

14. ABSTRACT
The BRI project aims to investigate the use of novel nano-optoelectronic systems based upon twodimensional (2D) heterostructures to realize breakthrough technologies for optical communications. The 2D heterostructure devices feature atomically-thin transition metal dichalcogenides (TMDs) and black
phosphorous, in combination with graphene and boron nitride. During this award period, we have made exciting progress towards the objective, including material innovation, device engineering, and development and investigation of 2D optoelectronics and integration with nano-photonic structures. In specific: (1) We have developed layer by layer growth of a wide range of TMDs by both MBE and physical vapor transport. (2) We have developed both TMD based optoelectronic devices near visible wavelength range and black-phosphorus based mid-infrared optoelectronics. These devices include light emitting diodes (LEDs), nano-cavity integrated monolayer LEDs, 2D heterostructure LEDs, optical and electrical driven single quantum emitters in monolayer WSe2, and mid-Infrared black phosphorus photodetector with electrical control; (4) development of novel materials and device concepts, such as the discovery of 2D topological insulators for low energy dissipation devices.

15. SUBJECT TERMS
2-D Heterostructures, Nanophotonics, Nano-Optoelectronics, graphene

16. SECURITY CLASSIFICATION OF:			17. LIMITATION OF ABSTRACT	18. NUMBER OF

a. REPORT	b. ABSTRACT	c. THIS PAGE		PAGES	19a. NAME OF RESPONSIBLE PERSON
Unclassified	Unclassified	Unclassified	UU		POMRENKE, GERNOT
					19b. TELEPHONE NUMBER *(Include area code)* 703-696-8426

AFOSR-BRI Final Report

Award Information

Project title: 2D (Two Dimensional) Heterostructures for Integrated Nano-Optoelectronics

Award number: FA9550-14-1-0277

Report date: 11/13/2017

Period covered by the report: Sept. 15 2014 – Sept. 14 2017.

Principle Investigator: Xiaodong Xu (Department of Physics, Department of Material Science and Engineering, University of Washington, Seattle, WA 98195)

Email: xuxd@uw.edu; phone: 206-543-8444

Co-PI: David Cobden (U. Washington), Fengnian Xia (Yale), Di Xiao (Carnegie Mellon), Zhixun Shen (Stanford), Mo Li and Steven Koester (Minnesota)

Program Manager: Gernot Pomrenke, Email: gernot.pomrenke@afosr.af.mil

Abstract

The BRI project aims to investigate the use of novel nano-optoelectronic systems based upon two-dimensional (2D) heterostructures to realize breakthrough technologies for optical communications. The 2D heterostructure devices feature atomically-thin transition metal dichalcogenides (TMDs) and black phosphorous, in combination with graphene and boron nitride. During this award period, we have made numerous exciting progress towards the objective, including material innovation, device engineering, and development and investigation of 2D optoelectronics and their integration with nano-photonic structures. In specific: (1) We have developed layer by layer growth of a wide range of TMDs by both MBE and physical vapor transport. (2) We have developed both TMD based optoelectronic devices near visible wavelength range and black-phosphorus based mid-infrared optoelectronics. These devices include light emitting diodes (LEDs), nano-cavity integrated monolayer LEDs, 2D heterostructure LEDs, optical and electrical driven single quantum emitters in monolayer WSe_2, and mid-Infrared black phosphorus photodetector with electrical control; (4) development of novel materials and device concepts, such as the discovery of 2D topological insulators for low energy dissipation devices. The success of our program will lead to disruptive optical technologies for long and short-distance communication, with low power, high density, and high bandwidth for both civilian and military needs.

Research Accomplishment

The objective of our BRI is to investigate the use of novel nano-optoelectronic systems based upon two-dimensional (2D) heterostructures to realize breakthrough technologies for optical communications. The 2D heterostructure devices feature atomically-thin transition metal dichalcogenides (TMDs) and black phosphorous, in combination with graphene and boron nitride. The success of our program will lead to disruptive optical technologies for long and short-distance communication, with low power, high density, and high bandwidth for both civilian and military needs. During this award period, we have made numerous exciting progress towards the objective, including material synthesis, device fabrication, and development of cavity-integrated 2D optoelectronics. In specific: (1) Material Growth: The progress in MBE growth includes layer by layer growth of 2H-WSe2 thin films from 1 ML to 8 ML, 1T'-WSe2, monolayer NbSe2, SnSe2 film on graphene, and 1T' phase MoTe2 on graphene. We also developed new physical vapor transport growth system with individual sample and substrate temperature control. (2) Contact engineering: We have achieved very low-noise, non-hysteretic, ambipolar transistors from monolayers, bilayers and trilayers of WSe_2 using few-layer graphene contacts, both thin and think hBN dielectric, and local contact gating; (3) optoelectronic devices: We have made high quality monolayer WSe_2 light emitting diodes (LEDs), the first nano-cavity integrated monolayer LEDs, and 2D heterostructure LEDs and photodetectors; optical and electrical driven single quantum emitters in monolayer WSe_2; and Mid-Infrared black phosphorus photodetector with electrical control; (4) discovery of 2D topological insulators for low energy dissipation devices; (4) theoretical investigation of novel materials and device concepts. We have been working on theoretical understanding of valley-dependent phenomena, particularly optical effects, in both 2D Dirac materials and novel Dirac materials called 3D Weyl semimetals. The team has total 41 journal publications.

Our team has also published several high impact review papers. For instance, Refs. [1-3] extensively discuss the status and the future of 2D materials including graphene, TMDs, black phosphorus and their various heterostructures in optoelectronics, electronics and valleytronics. These papers have been extremely well recognized in 2D community and are receiving hundreds of citations every year. Another review paper "Black Phosphorus and Its Isoelectronic Materials" is also under revision (Ref.[4]). These review papers are playing and will continue to play an important role in the development of 2D optoelectronics and electronics.

A. Material Synthesis

We have made progress in material growth and characterization using both MBE and physical vapor transport techniques. The progress in MBE growth and characterization is led by co-PI **Shen**. We succeeded in over 10 different kinds of monolayer TMD growth to investigate the reduced dimensionality caused quantum properties, including 2H-$MoSe_2$, 2H-WSe_2, 1T'-$MoTe_2$, 1T'-WTe_2, $NbSe_2$. Combined with the ARPES, STM and theoretical calculations, versatile quantum properties are investigated. Progress including 1) Direct observation of the indirect to direct bandgap transition in monolayer TMD. **Shen** group is the first one to achieve large area $MoSe_2$ and WSe_2 growth with the precisely control of the layer number to reveal the detailed layer by layer electronic structure evolution. For instance, layer by layer growth of 2H-WSe_2 thin films from 1 ML to 8 ML is realized. The *in situ* ARPES measurements on monolayer to few layers directly traced the indirect to direct bandgap transition as well as a giant Rashba-type spin splitting with gap sizes of 180 meV and 475 meV in $MoSe_2$ and WSe_2, respectively. (2) Investigated the

excitonic effect of monolayer TMD. Collaborated with STM/STS group, the effect of prominently reduced screening in monolayer two-dimension TMDs has been investigated in $MoSe_2$. The quasi free-standing monolayer shows giant bandgap renormalization and excitonic effect in monolayer $MoSe_2$. (3) Investigated the CDW and Superconductivity state in the 2D limit: Shen group developed the growth of monolayer $NbSe_2$. With the collaboration with STM/STS and transport group, we investigated the evolution of CDW and superconductivity state in monolayer $NbSe_2$, as well as the CDW state in 1D mirror twin boundaries of monolayer $MoSe_2$.

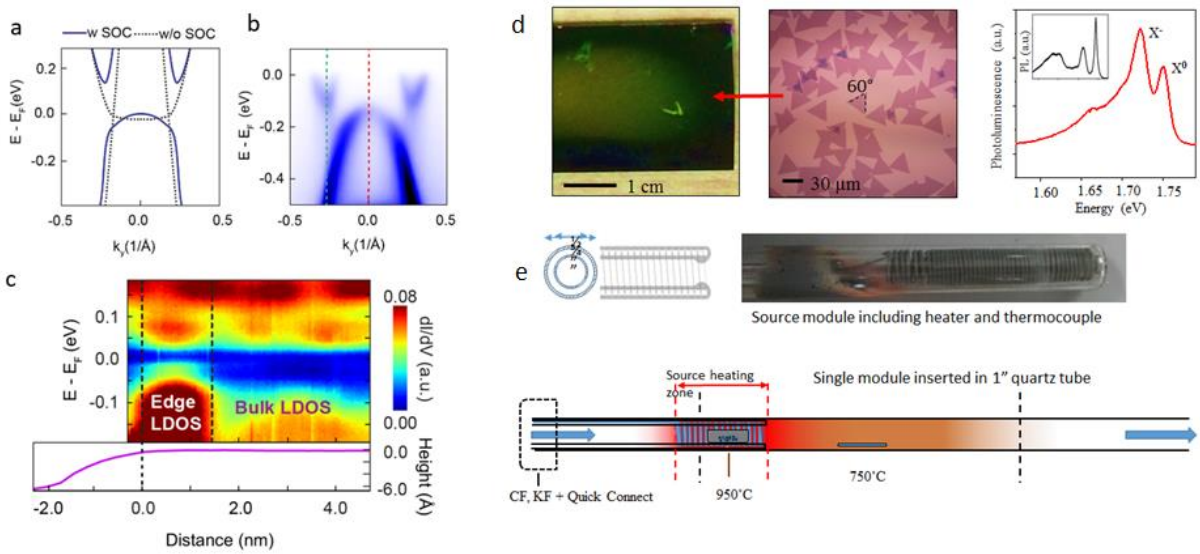

Figure 1. Progress in material synthesis. (**a**) Low energy calculation and (**b**) ARPES spectra show the bulk gap opening due to a strong spin-orbit coupling in monolayer 1T'-WTe_2. (**c**) Spatial STS mapping across the edge of a 1T'-WTe_2 domain observes the edge state inside the bulk gap. (**d**) Physical vapor transport growth results of monolayer WSe_2. (e) Scheme of new growth system.

In parallel to the MBE growth, **Cobden** and **Xu** have developed growth of high optical quality TMDs, whose optoelectronic properties at low temperature is comparable to the exfoliated samples (Fig. 1a). To achieve repeatable and controllable growth, we have developed new growth system (Fig. 1b). This powerful system enables the control of a wide range of growth parameters, including individual sample and substrate temperature, vapor pressure, time and cooling rate. The as-grown sample has been used to demonstrate monolayer nanocavity laser, monolayer light emitting diodes (LEDs), monolayer LED integrated with nanocavity, and electrically and optically pumped 2D single quantum emitters, as described in Section B.

B. TMD Heterostructure Optoelectronics

B.1 Monolayer and Heterostructure Light Sources and Detectors

(1) *Contact-Engineering:* It is of crucial importance to our envisaged technologies that a means needs to be established to produce robust electrical contacts, routinely, in non-trivial arrangements, with lithographic control, and in large arrays, to monolayer semiconductor materials. 2D semiconductors present unique challenges in this regard, thanks to pervasive Schottky barriers and complex, uncharacterized chemistry. **Cobden** and **Xu** have methodically tested a variety of

approaches, with emphasis on exploiting the strengths and unique features of 2D materials, such as the ability to perform very local electrostatic control and surface chemical treatments, and to incorporate 2D metals as the leads. **Cobden** and **Xu** have tried two approaches. We have already achieved very low-noise, non-hysteretic, ambipolar transistors from monolayers, bilayers and trilayers of WSe_2 using few-layer graphene contacts, think hBN dielectric, and local contact gating (Fig. 2). In the second approach, we created tunneling contacts made all by 2D materials: graphene as metal contact (top layer), mono or bilayer BN as tunneling barrier (middle), and monolayer WSe2 (bottom). Using this tunneling geometry, we are able to realize an ambipolar transistor and the electrical performance does not change as a function of temperature due to the carrier tunneling nature.

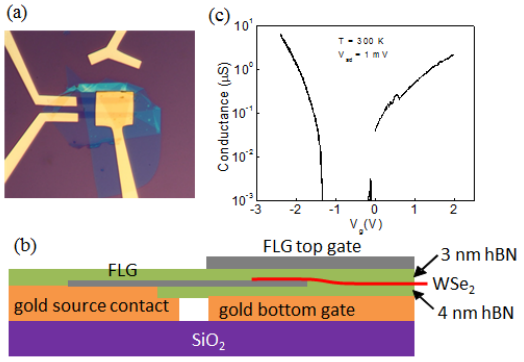

Figure 2. **Contact engineering**. (a) Optical microscope image and (b) schematic of monolayer WSe_2 ambipolar transistor based on dual-gated graphene contacts. (c) Ambipolar transport data.

(2) *Cavity-integrated light source*: Using the developed tunneling contact technologies, we have realized monolayer WSe_2 LEDs with very sharp excitonic features (Figs. 3a-c). Tuning the bias current enables the electroluminescence from different excitonic states, such as positively and negatively charged excitons as well as neutral excitons. **Xu** and **Cobden** have further developed fabrication technologies to integrated monolayer LEDs with GaAs photonic crystal cavity. Figure 3d shows hybrid WSe_2/GaP photonic crystal cavity device with cavity-enhanced EL from WSe_2 at room temperature and 1 MHz direct modulation of the EL[5]. In addition to electrically pumped light source, the Xu group created a photonic crystal nano-cavity laser using monolayer WSe_2 as a gain material[6] (Figs. 3e-g). A continuous-wave nanolaser operating in the visible regime is achieved with an optical pumping threshold as low as 27 nanowatts at 130 K, similar to the value achieved in quantum-dot PCC lasers. The key to the lasing action lies in the monolayer nature of the gain medium, which confines direct-gap excitons to within one nanometre of the PCC surface. Our developed cavity-integrated 2D material technologies will be used in developing ultra-low power optoelectronic devices due to the enhanced light-matter interaction. The developed technology will

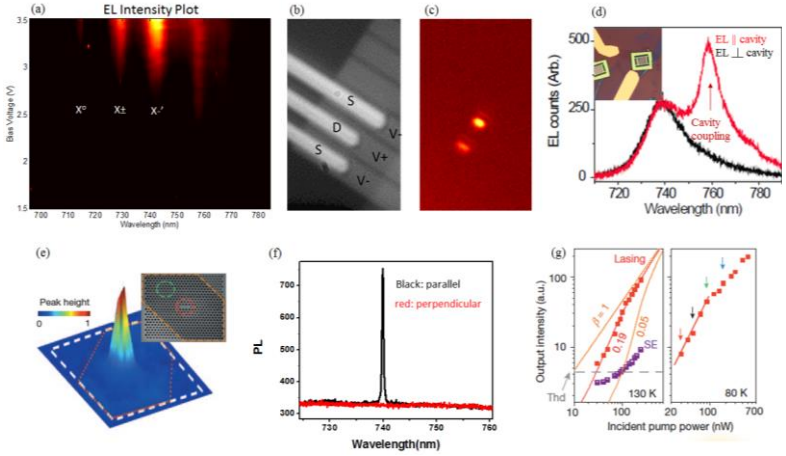

Fig. 3. Cavity integrated monolayer light sources. (**a**) Electroluminescence (EL) intensity plot of a monolayer WSe_2 LED as a function of bias and emission wavelength. (b) SEM (c) EL image of the device. (d) Polarization resolved EL of a cavity integrated monolayer WSe_2 LED. (e) PL image of monolayer WSe_2/GaP photonic crystal cavity. (f) Polarization resolved PL showing cavity coupled monolayer PL. (g) power dependent PL signifies lasing.

be useful for building energy efficient devices including, modulator, optical switch as well as detector.

(3) *Heterostructure p-n junction optoelectronics*: Recent advances in assembly techniques for van der Waals heterostructures has enabled the band engineering of semiconductor heterojunctions for atomically thin optoelectronic devices. We have demonstrated a $WSe_2/MoSe_2$ heterostructure optoelectronics. In such a heterostructure, type II band alignment forms, where the lowest energy conduction is in monolayer $MoSe_2$ while the highest energy valence band in WSe_2. Interlayer excitons can form in the heterostructure, where Coulomb-bound electrons and holes are confined to opposite layers. The interlayer exciton have shown promising properties for novel excitonic devices, including a large binding energy, micron-scale in-plane drift-diffusion, and long population and valley polarization lifetime. We demonstrate interlayer exciton optoelectronics based on electrostatically defined lateral p-n junctions in a $MoSe_2/WSe_2$ heterobilayer (Fig. 4). Applying a forward bias enables the first observation of electroluminescence from interlayer excitons. At zero bias, the p-n junction functions as a highly sensitive photodetector. We performed photocurrent measurement as a function of light excitation energy, i.e. photocurrent spectroscopy. We observe a resonance feature near interlayer exciton PL, which is the direct observation of resonant optical excitation of the interlayer exciton. In addition, the resulting photocurrent amplitude from the interlayer exciton is about 200 times smaller compared to the resonant excitation of intralayer exciton. Since the photocurrent amplitude is proportional to photo-excited exciton population, this suggests that interlayer exciton oscillator strength is two orders of magnitude smaller than that of the intralayer exciton. This is consistent with the fact that the spatial separation of electron and hole to opposite layers reduces the exciton dipole moment. These results lay the foundation for exploiting the interlayer exciton in future 2D heterostructure optoelectronic devices.

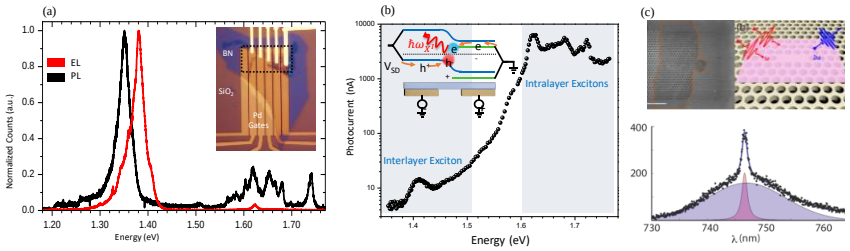

Figure 4. (a) EL spectrum (red) overlaid with PL spectrum (black) of a $MoSe_2/WSe_2$ heterostructure. Inset: optical microscope image. (b) Photocurrent spectroscopy of the heterostructure p-n junction resolves the resonant excitation of interlayer exciton. (c) Cavity enhanced second harmonic generation from a monolayer WSe_2.

(4) *Cavity-enhanced second-harmonic generation*: While digital optical computing may never outperform an electronic computer, computing paradigms such as neuromorphic computing that rely more on communication will benefit from optical implementation. Unfortunately, while optics offer an extremely high level of parallelism, the main bottleneck remains the weak nonlinearity. Here, we take the first step in exploiting nonlinearity from monolayers by integrating with a nanocavity. In collaboration with **Majumdar**, **Xu** have demonstrated enhanced SHG from monolayer WSe_2 by integrating with a photonic crystal cavity (Fig. 4c). The fundamental mode of the cavity is near telecom wavelength. By exciting the system with a laser pulse near 1.5 μm, we observe a sharp peak in the second harmonic spectrum (Fig. 4c, bottom). This sharp feature is the evidence of cavity enhanced second harmonic generation.

(5) *Multi-Modal MoS_2 Photodiodes/Phototransistors*: **Koester** has demonstrated a multimodal 2D material photodetector platform which uses both a lateral field-effect transistor (FET) structure for high optical gain and a vertical photodiode structure, which allows large-area detection and produces fast optical response[7]. This platform, shown in Figure 5a, consists of a multilayered TMD material such as MoS_2 or WSe_2 which is assembled directly on top of prefabricated electrodes, and a transparent ionic liquid which is used as a top-gate electrode. The channel region between the electrodes operates as a phototransistor with lateral transport, while the electrode region operates as a vertical Schottky photodiode device. We used scanning photocurrent microscopy (SPCM) measurements to confirm the device operation, and showed that photocurrent generation in the channel region and the electrode region are governed by a photogating (PG) and a photovoltaic (PV) mechanisms, respectively. For a device using a WSe_2 channel, and using an incident wavelength of 532 nm, we demonstrated that the high gain operation mode can produce responsivities as high as 1270 A/W in PG mode, while in PV mode external quantum efficiency as high as 48.5% under zero bias conditions was demon-strated (Figure 5b). The characteristics of each mode were shown to be dynamically tunable by changing the gate and drain voltages on the device.

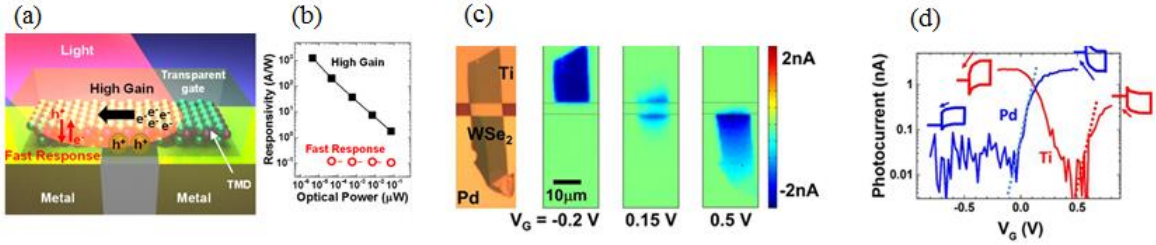

Figure 5. (**a**) Diagram of multi-model TMD photodiode/phototransistor. (**b**) Responsivity of a WSe_2 device operating at 532 nm. In the high-gain mode, responsivities as high as 1270 A/W were demonstrated. (**c**) Optical image of a WSe_2 flake assembled on Ti and Pd electrodes along with photocurrent maps at $V_D = 0$ for different values of V_G. (**d**) Semilog plots of photocurrent amplitude vs V_G on both Ti and Pd electrodes at $V_D = 0$. The relative Schottky barrier height difference of 0.6 V can be determined by the shift of forward bias turn-on which is indicated by the dashed lines.

A further interesting outcome of this device geometry, is that it allows for a determination of the Schottky barrier height of different metal electrode materials relative to the 2D material. As shown in Fig. 5c, we performed photocurrent measurements (in PV mode) on WSe_2 flakes with Pd and Ti electrodes. A comparison of the photocurrent on the two metals (Fig. 5d) showed an offset of 0.6 V between the forward bias current in these two devices, indicating an offset of 0.6 V in the Schottky barrier heights between Pd and Ti.

B.2 Single Quantum Emitters in 2D Semiconductors

(1) *Single quantum emitters in 2D semiconductors*: Solid state emitters are important for developing novel quantum technologies. The **Xu** group has demonstrated a new class of single quantum emitters (SQEs) based on excitons that are spatially localized by defects in 2D WSe_2 monolayers[8] (Fig. 6a). The optical emission from these SQEs shows narrow linewidths of ~130 μeV. Second-order correlation measurements revealed a strong photon antibunching, which unambiguously established the single-photon nature of the emission (Fig. 6b). The SQE emission shows two non-degenerate transitions, which are cross-linearly polarized (Fig. 6a). We assign this fine structure to two excitonic eigenmodes whose degeneracy is lifted by a large ~0.71 meV coupling, probably because of the electron–hole exchange interaction in the presence of anisotropy.

Magneto-optical measurements also reveal an exciton *g* factor of ~8.7, several times larger than those of delocalized valley excitons. In addition to their fundamental importance, establishing new SQEs in 2D quantum materials could give rise to practical advantages in quantum-information processing, such as an efficient photon extraction and a high integratability and scalability.

(2) *Single defect light emitting diode of a monolayer semiconductor*: In additon to optically-pumped single quantum emitters, we have fabricate LED structures for realization of electrically pumped single quantum light soucres[9]. We have engineered two complementary device structures by mechanical transfer process to stacking multiple monolayers on top of each other. The first, a vertical heterostructure design, allows spatial mapping of electroluminescence (EL) from intrinsic and defect-bound excitons over a large device area. The second type of LED relies on a p-i-n junction laterally defined within a WSe_2 monolayer, leading to EL primarily from single defects isolated in the narrow junction area. Figure 6c shows EL from three defects present in the lateral junction, with linewidths <300 μeV and a doublet structure, with consistent ~ 0.7 meV energy splitting. This EL spectra is consistent with PL sepctra in Fig. 6a, demonstration of the realization of electrical-driven 2D single quantum emitters.

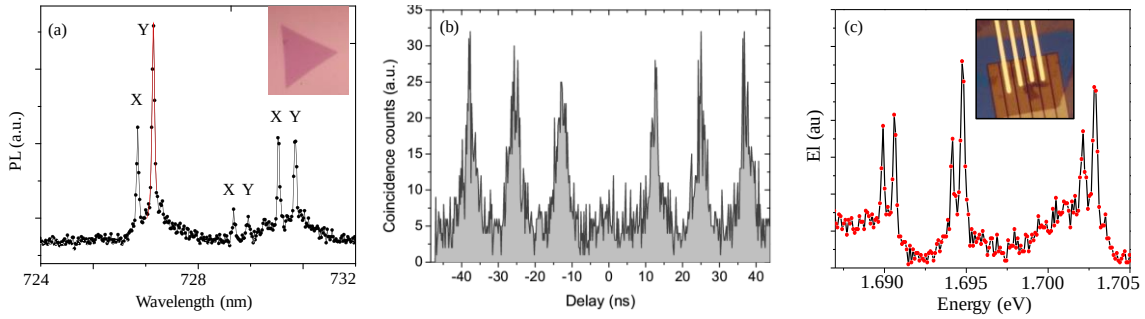

Figure 6. 2D single quantum emitters. (**a**) PL spectrum shows three pairs of defect bound exciton emission. Inset: optical microscope image of the sample. (**b**) Observation of photon-antibunching – hallmark of single quantum emitters. (**c**) EL spectrum for a lateral LED device showing emission from three single defects. Inset: Optical image of a lateral LED device.

C. Black Phosphorous Optoelectronics

During the period of the BRI project, **Li**, **Xia**, and **Koester** has been focusing on a newly emerged 2D material, namely, black phosphorus (BP). Its narrow, direct bandgap as low as 0.3 eV in multilayers is an ideal match for infrared applications. Our research efforts range from BP synthesis[10], to investigate its fundamental electronic and optical properties, and to develop integrated BP optoelectronic devices[11,12]. Highlight research results obtained by our effort are summarized below.

(1) *Lateral Heterostructures in Black Phosphorus*: The **Koester** group has developed a high spatial resolution, thinning method for realizing lateral black phosphorus (BP) heterostructures[13]. This process utilizes a cyclic technique involving BP surface oxidation and vacuum annealing to create BP flakes as thin as 1.6 nm (3 layers). The process also uses a spatially patternable Al_2O_3 mask which protects the BP region underneath from etching, thereby allowing the creation of lateral

heterostructures with spatial resolution as small as 150 nm. Examples of the thinning process spatial patterning are shown in Figure 7. This thinning/patterning technique was shown to proceed in a layer-by-layer fashion with a single monolayer being removed after each exposure and annealing cycle.

We also characterized the optical properties of the thinned BP films. Raman peaks from BP could be observed for flakes thinned down to 1.6 nm (3 layers). Furthermore, we showed that photoluminescence (PL) at near-infrared wavelengths could be observed in BP thinned using our cyclical process. PL with a peak emission wavelength around 990 nm was observed in a flake thinned from 7 nm down to 2 nm (4 layers).

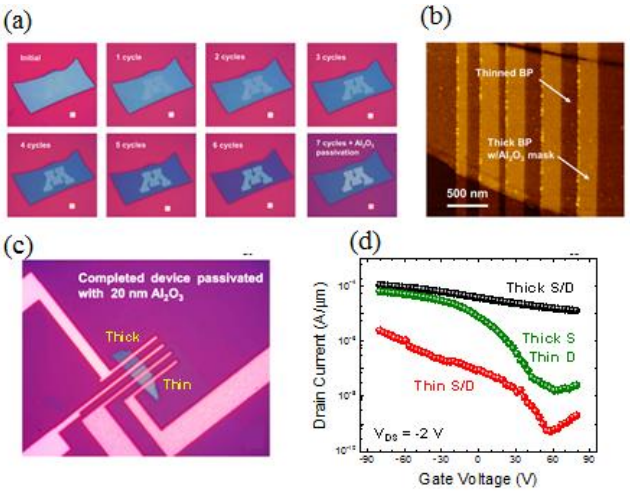

Figure 7. (**a**) Optical micrographs of a patterned BP sample after each thinning cycle. The UMN logo region is passivated with Al_2O_3 and the other flake regions are thinned in a cyclical manner, evident by the change in color/contrast. (**b**) AFM micrograph of patterned BP flakes with sub-150 nm features. (**c**) Optical micrograph of a BP lateral heterostructure MOSFET. (**d**) I_D vs. V_{GS} measurements of heterostructure MOSFET showing optimized performance in the heterostructure configuration, which provides 1000× improvement in ON/OFF current ratio with only slight degradation in ON current.

Finally, we used the thinning process to create lateral heterostructure field-effect transistors (FETs). In these device, shown in Fig. 7c, contacts were first made to a thick BP flake. Then, a portion of the BP flake was thinned using our cyclical process. Next, contacts were made to the thinned region and finally the entire device was passivated. The contacts were arranged so that the characteristics of the thick, thin and heterostructure regions could be measured independently. The results of a typical heterostructure FET are shown in Fig. 7d with thick and thin regions of 12 nm and 8 nm, respectively. The figure shows the device with thick source/drain (S/D) regions had high ON current, but poor turn-off behavior. The thin S/D device showed improved on-to-off current ratio, but had low ON current. However, the device where the thick source and thin drain showed drive current similar to the thick-only device, but 1000× improved ON/OFF current ratio. This technique has the potential to be applied to a wide range of devices, included heterostructure MOSFETs, TFETs and optoelectronic devices.

(2) *Black Phosphorus MOSFETs and TFETs*: The **Koester** group also performed a comprehensive analysis of the effect of thickness, temperature, and source–drain bias voltage, V_{DS}, on the subthreshold slope, *SS*, and off-state properties of Schottky-contacted BP FETs[14]. Locally back-

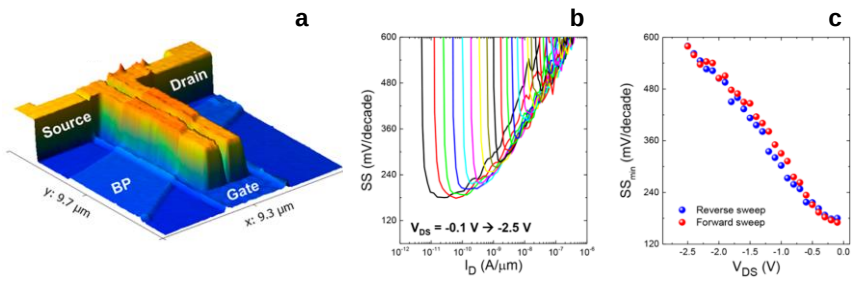

Figure 8. (**a**) Three-dimensional AFM height map of a typical locally backgated BP MOSFET. (**b**) Subthreshold slope, SS, vs drain current, I_D for increasing values of source-to-drain bias, V_{DS}. (**c**) Minimum subthreshold slope, SSmin, vs V_{DS} for the same device as in (a).

gated p-MOSFETs (Fig. 8a) with thin HfO_2 gate dielectrics were analyzed using exfoliated BP layers ranging in thickness from ~4 to 14 nm. The *SS* was found to degrade with increasing V_{DS}, as shown in Fig. 8b and c, with the effect being stronger as the BP channel thickness increased. We also found that *SS* degraded as the BP thickness was increased, with the degrading stronger at high V_{DS}. Modeling showed that the subthreshold degradation was a result of charge injection from the drain contact, and provide guidance on how to achieve ideal *SS*, by using thin BP and near band-edge contacts.

We also have fabricated and demonstrated the operation of BP tunneling FETs (TFETs) with transport directions aligned along the armchair and zigzag crystal orientations using a triple-gate device structure as shown in Fig. 9a[15]. This structure allows the realization of electrostatically-doped source and drain electrodes, which allow the observation of true band-to-band tunneling, as opposed to injection from a Schottky contact.

Using this structure, strong (~10^3) band-to-band-tunneling anisotropy can be observed between the two crystal orientations as shown in Fig. 9b. The current-voltage behavior of these devices was also analyzed at low drain bias in order to determine the limits of the subthreshold performance.

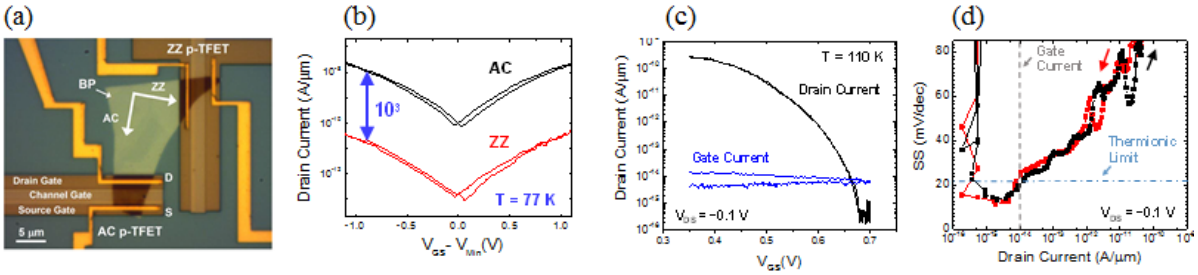

Figure 9. (a) Optical micrograph if triple-gated BP structure with transport in the armchair (AC) and zigzag (ZZ) directions. (b) I_D vs. V_{GS} at high drain bias in the AC and ZZ directions at T = 77 K. Anisotropy of 10^3 is observed as a result of the effective mass difference in the two crystal directions. (a) Drain current vs. gate voltage at T = 110 K for a BP p-TFET. (b) Subthreshold slope vs. drain current for the same device as in (a). The device shows SS_{min} = 22 mV/decade, near the subthermionic limit at this temperature.

Fig. 9c shows the results of a TFET with *SS* near to the thermionic limit before the onset of gate leakage current. A value SS_{min} = 22 mV/dec was achieved at T = 110 K (Fig. 9d), a step towards realizing steep-slope BP-TFETs.

(3) *Black Phosphorus Avalanche Photodiodes*: The **Koester** group has performed preliminary experiments to evaluate the potential of BP for use in avalanche photodiodes (APDs). Figure 10a shows current voltage characteristics of BP photodiodes illuminated at λ = 532 nm under high bias operation. The extracted external and internal quantum efficiencies (EQE and IQE) as a function

of bias at an optical power of 19.1 μW are shown in Fig. 10b. The results show substantial gain that increases with bias voltage, which could provide possible evidence of avalanche multiplication.

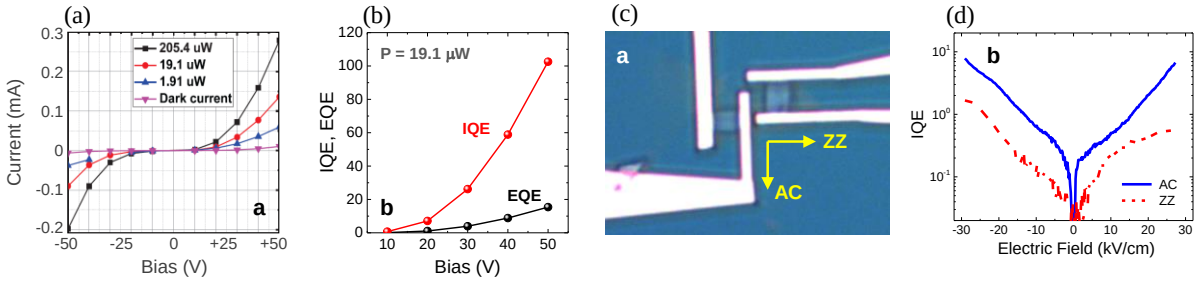

Figure 10. (**a**) I-V curve for a BP photodiode at different optical powers and λ = 532 nm. (**b**) IQE and EQE vs. bias for same device as in (a). (**c**) Optical micrograph if right-angle photodetector devices. (**d**) Extracted IQE for photodiodes in (a) oriented along the AC and ZZ directions.

We also characterized the photocurrent dependence on orientation at high bias voltages in BP photodiodes. These measurements were performed using etched, right-angle photodetector structures as shown in Fig. 10c to characterize photocurrent along the AC and ZZ directions. As shown in Fig. 10d, we found a 5-10× increase in photocurrent for devices with the transport direction along the AC vs. the ZZ direction. The AC-oriented devices also achieved optical gain at a lower applied electric field compared to the ZZ orientation, another possible indication of avalanche gain. Additional measurements are ongoing to confirm the origin of the gain mechanism and to extract the electron / hole ionization coefficients.

(4) *Mid-infrared black phosphorus photodetector and Electro-Optical Modulation***:** Sensing and detecting electromagnetic radiations at mid-infrared (MIR) wavelength (2-20 μm) is of great importance for a number of applications. For example, the MIR regime covers the thermal emission of most biological and mechanical systems, making it a critical wavelength range for thermal imaging and heat scavenging applications. MIR spectroscopy has also been regarded as the golden standard for identifying various bio/chemical molecules through their vibrational fingerprints. Despite its great significance, the chip-scale mid-IR photonic system operating at room temperature is less developed mainly because of the lack of high quality MIR active materials, which can be readily integrated with MIR waveguides and other optical components.

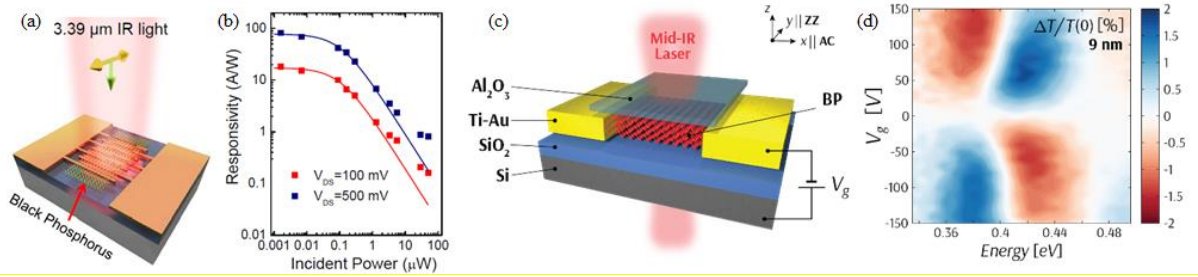

Figure 11. (**a**) A schematic view of the BP mid-infrared photodetector. (**b**) The external responsivity versus incident power at 3.39 μm under biases of 100 and 500 mV, respectively. (**c**) Schematic illustration of the BP modulator, featuring the normally incident mid-IR laser beam and the heavily p-doped silicon substrate as the back gate. The BP flake is oriented with the arm-chair (AC) crystalline axis along the x-axis and the zig-zag (ZZ) crystalline axis along the y-axis. (**d**) The modulation level measured as functions of energy and gate bias for 9nm thick BP. Three characteristic peaks can be observed at E_a =0.38 eV, E_b =0.43 eV and E_c=0.5 eV.

Black phosphorus (BP) recently joined the family of layered materials[16]. Both **Xia** and **Li** demonstrated its unique potential in high performance optoelectronics in the MIR regime. Specifically, BP in its thin film form has a moderate bandgap around 0.3 eV, which not only ensures the strong MIR light-matter interaction, but also allows for suppressed dark current and the low noise photodetection that cannot be achieved in gapless graphene[16]. In addition, the appealing transport characteristics such as high carrier mobility at room temperature also enable the efficient collection of photocarriers. We demonstrated a room temperature BP metal-semiconductor-metal (MSM) MIR photodetector that exhibits a high external responsivity of up to 82 A/W at 500 mV voltage bias and a high photoconductive gain at 3.39 μm when the incidence light power is low. The key results are summarized in the Figs. 11 a&b. The noise measurements further validate that the device is capable of detecting low intensity mid-IR light down to pico-watt even at room temperature. As an interesting and important feature of BP, we show that its low-crystalline symmetry can also give rise to a photoresponse sensitive to the incident light polarizations. This unique property can be harnessed for applications in which light polarization can reveal additional information, such as sensing and imaging in hazy/foggy conditions[17].

We further demonstrate electro-optic modulation of mid-IR absorption in few-layer black phosphorus under field applied by an electrostatic gate, as shown in Fig. 11 c&d[18]. Our experimental and theoretical results find that, within the doping range obtainable in our samples, the quantum confined Franz-Keldysh effect is the dominant mechanism of electro-optic modulation. Spectroscopic study on samples with varying thickness reveals strong layer-dependence in the inter-band transition between different sub-bands. Using a 9 nm thick BP layer, the modulation level of the transmission reaches 5%. Compared to traditional narrow-bandgap semiconductors widely used in MIR detection, such as mercury cadmium telluride (MCT) and indium arsenide (InAs), BP offers tremendous flexibility in heterogeneous integration with various photonic structures such as optical waveguides and cavities, making it a viable material in monolithic MIR photonic systems for on-chip spectroscopy and the imaging applications.

(5) *hBN/black arsenic phosphorus (b-AsP) heterostructures*: **Xia** leveraged black arsenic phosphorus (b-As_xP_{1-x}), an isoelectronic material of BP to enable light-matter interaction at wavelengths much longer than the cut-off wavelength of BP, which is around 3.7 μm. Our collaborator in Germany, Prof. Nilges is responsible for the synthesis of b-AsP. Introduction of arsenic into BP allows the tuning of the bandgap from 0.33 to around 0.15 eV. Most importantly, we fabricated mid-infrared (MIR) photodetector based on hexagonal boron nitride (hBN)/b-As_xP_{1-x}/hBN heterostructures and showed that such photodetectors are highly stable in the long run. No performance degradation was observed up to a few months. The b-As_xP_{1-x} photodetector ($x=0.81$ in this device) schematic is shown in the Fig. 12a and the inset of Fig. 12b shows the cross-section view of the photo-active region and the corresponding elemental mapping. The polarization-

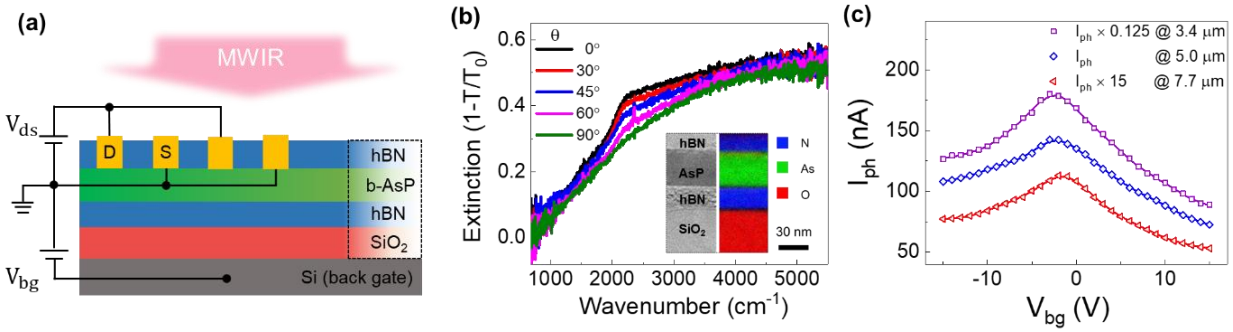

Figure 12. (a) A schematic view of the hBN/b-AsP/hBN heterostructure photodetector. (b) The infrared extinction spectra of the b-AsP under different polarizations of the incident light. Inset: cross-section view of the hBN/b-AsP/hBN heterostructure (left) and the elemental mapping of the heterostructure cross-section (right). (c) The extrinsic responsivity for 3.4, 5.0 and 7.7 μm incident light as a function of the backgate bias, respectively.

resolved infrared extinction spectra of the b-AsP material are shown in Fig. 12b. The absorption edge is at around 1000 cm^{-1}, corresponding to a bandgap of 0.124 eV. In the demonstrated b-AsP photodetector, the b-AsP photoactive layer is completely protected from oxidation by the hBN encapsulation (no O in elemental mapping), which also eliminates the surface trap states. Distinguished from other recent demonstrations on black phosphorus and b-AsP, our MIR photodetectors based on hBN/b-AsP/hBN heterostructures work in the intrinsic photoconductive mode, allowing for the high-speed operation. The photocurrent reaches the maximum at the charge neutral point (Fig. 12c) where the photo-carriers have the longest lifetime, showing the room-temperature extrinsic responsivity of 320, 24.7, and 1.03 mA/W at 3.4, 5.0, and 7.7 μm, respectively. We estimate the 3-dB cut off frequency of the photoconductor to be around 11.6 GHz. The decent room-temperature responsivity at MIR, together with high operational speed and long-term stability, makes b-AsP promising in MIR applications, such as thermal imaging, biomedical sensing and even mid-infrared optical communication. Our MIR photodetectors were characterized all at room temperature, making them suitable for portal devices without costly cryogenic accessories. If compared with micro-bolometer based MIR detectors, the intrinsic photoconductive effect in our b-AsP makes the photodetector operational at much higher frequencies beyond 10 GHz. Furthermore, the layered structure of b-AsP makes its integration with other optical structures easy. As a result, our b-AsP photodetectors can be incorporated with sub-systems readily. These results are summarized in Ref.[19], which is being submitted for publication now.

(6) *Time-resolved photocurrent measurement of BP photodetectors*: With its high mobility, narrow bandgap, and unique anisotropy, black phosphorus (BP) is a promising material for optoelectronic applications. To truly be competitive, however, BP photodetectors must reach speeds of tens of GHz. **Li** employed BP's nonlinear photoresponse to measure the intrinsic speed of a BP photodetector using ultrafast pump-probe measurements, as shown in Fig. 13. With this technique, we are able to observe how the detection speed depends on both the incident power and applied

source-drain bias [20]. A minimum response time of 60 ps was observed which corresponds to an intrinsic bandwidth of 9 GHz. This response speed is limited by the time it takes for carriers at the

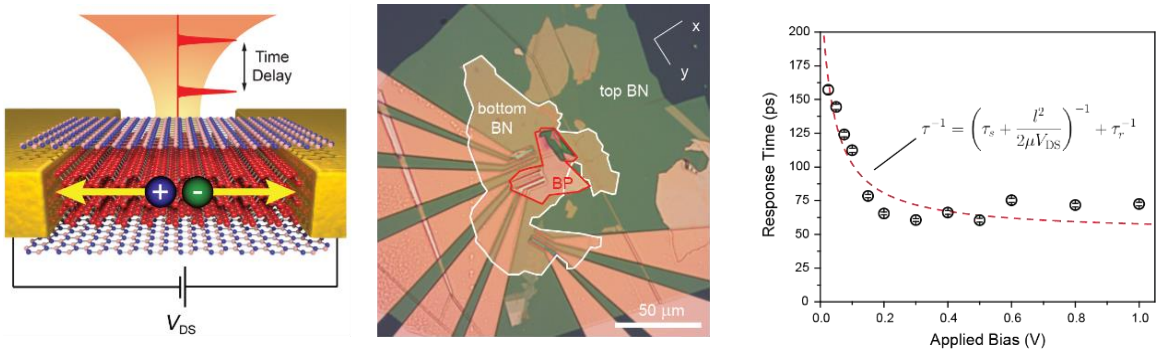

Figure 13. (Left) Illustration of device and measurement scheme. Ultrafast pulses excite photocarriers which are swept to the contacts with an applied bias. (Middle) Optical microscope image of completed device. Black phosphorus (BP) is encapsulated with boron nitride (BN) which provides both passivation and a high quality substrate for improved mobility. Channel length is 1.5 μm. (Right) Response time as a function of source-drain bias. An increasing bias helps to sweep photoexcited carriers in the channel to the contacts and reduces the carrier lifetime in the channel. A minimum response time of 60 ps corresponding to a device bandwidth of 9 GHz was observed for a moderate bias.

center of the channel to diffuse close enough to the contacts to be influenced by the applied bias. Unlike Ohmic contacts to 3D materials, Schottky barriers are usually formed in 2D materials and other ultra-thin body devices which prevents the electric field from penetrating far into the channel. Therefore, this speed limitation can be potentially overcome by using graphene to electrically contact above and below the BP so that the field is vertical rather than in-plane. This has been demonstrated in MoS2 and WSe2 heterostructures.

(7) *Silicon photonics integrated BP photodetector in telecom band*: **Li** demonstrated the first BP infrared photodetector integrated on silicon waveguides (Fig. 14). This BP detector includes a top gate in a field-effect transistor configuration, enabling tuning the BP to different regimes of carrier concentration. With this technique, we determined that photocurrent generation is dominated by photovoltaic effect in the low carrier concentration regime and by photothermal effect in the high carrier concentration regime. By applying appropriate gate voltage to tune the BP in the optimal

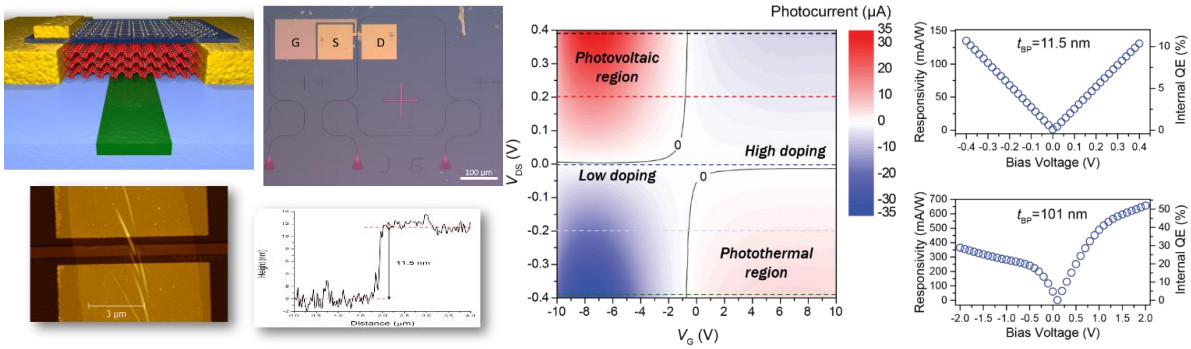

Figure 14. (a) Illustration, optical microscope and AFM images of BP photodetector integrated on silicon waveguides. b Photocurrent in BP photodetector as a function of gate voltage and source-drain voltage. Photovoltaic and photothermal regimes of carrier generation are identified. Responsivity up to 150 mA/W and 650 mA/W are achieved in 11.5 nm and 100 nm thick BP, respectively.

condition for photodetector, we achieved responsivity of 150 mA/W with ~11.5 nm thick BP and demonstrated optical communication with data rate at 3Gb/s. The responsivity improves to 650 mA/W when thicker BP flake is used. The results were published in Nature Photonics[21]. Considering both the responsivity and the speed, this device represents the best performance in all 2D material photodetectors published so far and also approaches the performance of commercial InGaAs photodetectors.

(8) *3D Integration of Black Phosphorus Photodetector with Silicon Photonics and Nanoplasmonics*: Despite of 2D materials' novel optoelectronic properties, their atomically thin geometry fundamentally limits the interaction cross-section with light and consequently the total achievable absorption or modulation of light is often inadequate for practical applications. Integration with planar photonic devices, such as silicon waveguides, can extend the interaction length in the 2D materials, but at the expense of larger device footprint, which can lead to increased energy consumption and reduced operation bandwidth. To circumvent such a trade-off, **Li** integrate BP with a plasmonic nanogap with a sub-diffraction width of 50-60 nm. In this nanogap, the optical field is highly concentrated and absorbed strongly with the BP to generate photocarriers efficiently. The BP layer and the plasmonic layer are integrated in 3D on top of silicon photonic waveguides and gratings, which delivers optical signal with low loss from fiber coupled signal sources. Fig. 15 illustrates the structure and displays the images of the actual device[22].

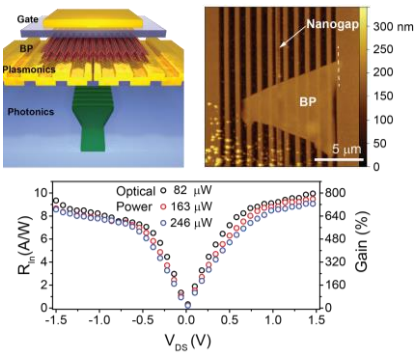

Figure 15. (Top-left) Schematic illustration of the 3D integrated BP photodetector on a silicon waveguide and a plasmonic nanogap resonator, which is also the contact to the BP. (Top-right) AFM image of BP and nanogap region of the device. (Bottom) The device has a photoconductive gain up to 800% and a responsivity of 10 A/W.

A very innovative design in this device is that the metallic plasmonic nanogap is also used as the source and drain contacts to the BP. Together with a top metal gate, the nanogap-BP forms a field effect transistor (FET) with a very short channel length of 50-60 nm. As a result, the carrier transit time in the channel is less than 50 ps, shorter than the measured carrier lifetime, allowing the photocarriers to circulate in the channeling multiple time before being recombined. When operated in the photoconductive mode, the BP photodetector can have a photoconductive gain greater than 800%, yielding an intrinsic responsivity as high as 10 A/W, as displayed in Fig. 15. This significant performance improvement stems from the novel co-integration of nanoplasmonics and 2D materials.

(9) *First Measurement of Third-Harmonic Generation (THG) in BP*: In addition to linear optical properties, the quantum confinement in 2D materials also leads to many novel nonlinear optical properties. For example, MoS_2, WSe_2, and hBN all with non-centrosymmetric lattice structures, have shown strong second-order nonlinear optical effects, such as second-harmonic generation (SHG). SHG in these materials has shown strong enhancement at the exciton resonances, can be electrically tuned by a local back gate,16 and has been utilized for optically probing the crystal orientation and thickness. Additionally, third-order optical nonlinearity such as third-harmonic generation (THG) has been observed to be strong in graphene, as well as in MoS_2 thin films. In terms of nonlinear optics in BP, its centrosymmetric crystalline structure only permits third-order nonlinearity but its strong anisotropy and layer dependent band structure should lead to very

intriguing nonlinear optical effects. Research to date, however, has been primarily limited to the saturable absorption effect in BP, studied with z-scan and ultrafast pump-probe techniques for liquid exfoliated BP suspensions and utilized for application in mode-locked lasers. The intrinsic optical nonlinearity of crystalline BP has not been experimentally investigated.

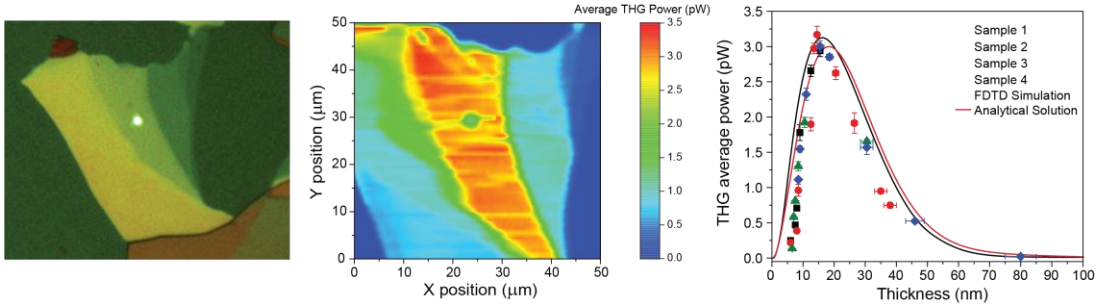

Figure 16. (Left) Image of the THG in BP as the green bright spot can be seen when the BP is illuminated with the pump laser of 1550 nm in wavelength. (Middle) Mapping of THG emission power over a BP sample with varying thickness. (Right) Due to interference effect of both the pump and the THG, the THG emission power strongly depends on the BP thickness (e.g. a sharp peak at 15 nm). Therefore, THG provide high contrast for imaging BP thickness.

In this effort, **Li** investigate BP's optical nonlinearity by measuring both the polarization and thickness dependence of THG in multilayer BP samples[23]. We find that the THG in BP is strong and highly dependent on both the polarization of the incident light and the number of layers under investigation, as shown in Fig. 16. From the measurement, BP's third-order nonlinear susceptibility is determined for the first time. It was found that the third-order susceptibility $\chi^{(3)}$ of BP is highly dependent on both the incident polarization and the number of layers present. The latter is related the resonance with the layer dependent structures of the sub-bands in BP and therefore can be utilized as a tool to probe the band-structures of BP.

D. New Directions

We have been developing new directions by both theoretical and experimental efforts in novel valley-dependent optical phenomena, 2D Dirac materials, 3D Weyl semimetals, photodetectors based on new perovskite heterostructures, and 2D topological insulators. Below is the description of selected research progress.

(1) *Optical generation and detection of pure valley current in TMDs*: Recent years have seen a surge of interest in the manipulation of the valley index of Bloch electrons, largely driven by its potential applications in electronics and optoelectronics. The valley index enumerates degenerate energy extrema

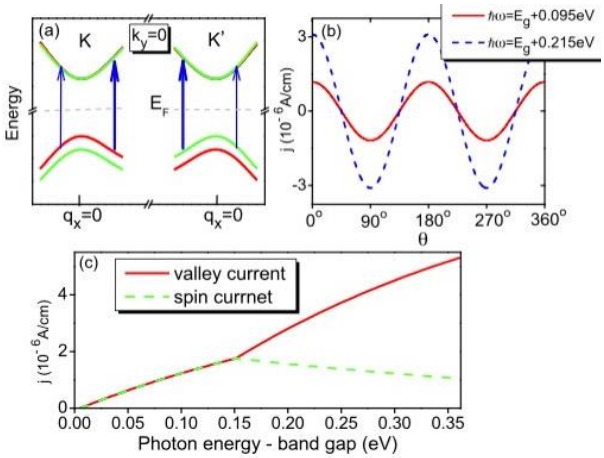

Figure 17. Linear valley and spin photogalvanic effect in monolayer TMD. (a) Schematics of band dispersion around valley K(K'). (b) Angular dependence of valley current on the polarization angle. (c) Valley/spin current as a function of photon energy (minus the band gap).

in momentum space. Such degeneracies are often present in two-dimensional (2D) materials with a honeycomblike structure, such as graphene, boron nitride, and transition-metal dichalcogenides (TMD). In these materials, weak intervalley scattering renders the valley index an effective degree of freedom that can be utilized in novel devices. This realization of valley-based electronics is called valleytronics, which depends crucially on the dynamical control of two quantities: valley polarization and valley current. **Xiao** and **Xu** have previously predicted that the valley polarization can be generated by circularly polarized light, which has subsequently been experimentally demonstrated in monolayer MoS_2. On the other hand, so far only valley-polarized electric current has been reported. In analogy to spintronics, it would be desirable to generate a pure valley current, in which there is no net motion of charge; carriers in the opposite valley move in the opposite direction. Such a pure valley current would prohibit any charge-related effect and generate minimal Joule heating, similar to a pure spin current (Fig. 17).

(2) *Magnetic ground states of two-dimensional magnetic semiconductors*: Layered transition-metal trichalcogenides with the chemical formula ABX3 have attracted recent interest as potential candidates for two-dimensional magnets. Using first-principles calculations within density functional theory, we investigate the magnetic ground states of monolayers of Mn- and Cr-based semiconducting trichalcogenides. **Xiao** show that the second and third nearest-neighbor exchange interactions (J2 and J3) between magnetic ions, which have been largely overlooked in previous theoretical studies, are crucial in determining the magnetic ground state. Specifically, we find that monolayer CrSiTe3 is an antiferromagnet with a zigzag spin texture due to significant contribution from J3, whereas CrGeTe3 is a ferromagnet with a Curie temperature of 106 K. Monolayers of Mn compounds (MnPS3 and MnPSe3) always show antiferromagnetic Neel order (Fig. 18). We identify the physical origin of various exchange interactions, and demonstrate that strain can be an effective knob for tuning the magnetic properties. Possible magnetic ordering in the bulk is also discussed. Our study suggests that ABX3 can be a promising platform to explore two-dimensional magnetic phenomena.

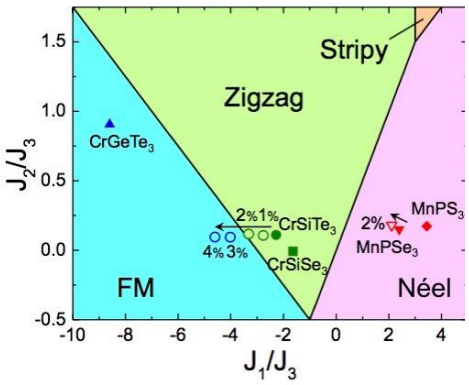

Figure 18. Phase diagram of the magnetic ground state of transition metal trichalcogenides monolayers.

(3) *Berry phase splitting of exciton energy spectrum*: The Berry phase of Bloch electrons and the topology of energy bands have attracted great attention in condensed matter physics. In the semiclassical picture, the Berry curvature, i.e., the Berry phase per unit area in the momentum space, manifests itself through an anomalous term in the group velocity of Bloch electrons, which can manifest in a number of transport phenomena such as the anomalous Hall effect and the spin Hall effect. Through the semiclassical quantization procedure, the Berry phase can also modify the energy spectrum. For example, the appearance of the zero energy Landau level observed in graphene can be understood as due to the Berry phase of pi around the Dirac point.

Recently, there has been intense interest in monolayers of transition metal dichalcogenides due to their extraordinary optoelectronic properties, and in particular, their giant exciton binding energy.

In these materials, the low-energy carriers behave like massive Dirac fermions with nonzero Berry curvature. Therefore they offer a perfect opportunity to study the Berry phase effect on excitons. Obviously, the Berry curvature will modify the relative motion of the electron-hole pair in an exciton (Fig. 19a). By quantitating the semiclassical dynamics, **Xiao** have found that the Berry curvature will modify the exciton Hamiltonian with an effective spin-orbit coupling term, which can cause an energy splitting between exciton states with opposite angular momentum. This splitting is determined by the Berry curvature flux through the k-space area spanned by the relative motion of the electron-hole pair. We also estimate this Berry phase induced energy splitting of excitons in transition metal dichalcogenides, a few tens of meV, which is consistent with previous numerical calculations and should be observable in future experiments.

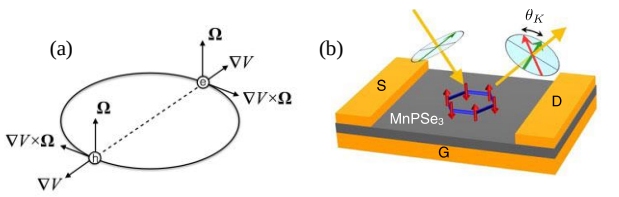

Figure 1. (a) Exciton motion in the presence of the Berry curvature. **(b)** Schematic of a magneto-optic device made from layered antiferromagnets.

(4) *Gate-Controllable Magneto-optic Kerr Effect in Layered Collinear Antiferromagnets*: Magneto-optic effects are one of the defining features of time-reversal (T) symmetry breaking in matter. Usually, the T symmetry is broken either by an external magnetic field or by the spontaneous appearance of a macroscopic magneti- zation such as in ferromagnets. Similar to their ferromagnetic counterparts, the T symmetry is also broken in antiferromagnets. However, because of their vanishing net magnetization one would naively expect an absence of magneto-optic effects in antiferromagnets. Using symmetry arguments and a tight-binding model, **Xiao** show that for layered collinear antiferromagnets, magneto-optic effects can be generated and manipulated by controlling crystal symmetries through a gate voltage. This provides a promising route for electric field manipulation of the magneto-optic effects without modifying the underlying magnetic structure. We further demonstrate the gate control of the magneto-optic Kerr effect (MOKE) in bilayer $MnPSe_3$ using first-principles calculations (Fig. 19b). The field-induced inversion symmetry breaking effect leads to gate-controllable MOKE, whose direction of rotation can be switched by the reversal of the gate voltage.

Our predicted gate-controllable MOKE has important implications in both fundamental research and practical applications. As the observed MOKE is very sensitive to the underlying magnetic order, it can be used to identify the magnetic ground state. Not only can this method distinguish between ferromagnets and antiferromagnets, but it can also be used to distinguish among different antiferromagnetic orders, such as Néel, zigzag, and stripy order on a honeycomb lattice, supplemented by symmetry analysis and band structure calculations. This is especially valuable for 2D materials since neutron scatter- ing is ineffective for these materials due to the small scattering cross section. Furthermore, the sensitivity of the MOKE to the magnetic order can be exploited for magnetic information storage. For instance, the reversal of the Néel vector will result in a change of sign of the observed MOKE. Thus, the information encoded in the Néel vector can be extracted using this gate-controlled MOKE in antiferromagnets.

(5) *Graphene-2D perovskite heterostructure phototransistors*: Graphene photodetectors are appealing for high-speed operation, broadband photo-absorption and their ease integration with silicon photonic systems. However, graphene photodetectors suffer from low responsivity (at order

of mA/W) due to their weak light absorption and ultrafast electron-hole pair recombination. In this project **Xia** showed that by integrating graphene photo-transistor with a two-dimensional (2D) perovskites $(BA)_2(MA)_{n-1}Pb_nI_{3n+1}$ heterostructure as shown in Fig. 20a, we can achieve a high responsivity well-beyond 10^3 A/W, which is significantly larger than that in graphene photodetectors (~ mA/W). Here, $BA^+ = CH_3(CH_2)_3NH_3^+$, $MA^+ = CH_3NH_3^+$ and the integer *n* is the number of lead iodide octahedral layers between two BA^+ organic spacers.

The high responsivity achieved in our heterostructure perovskites-graphene integrated photodetector can be twofold. Firstly, by using an atomically smooth hexagonal boron nitride (hBN) as the substrate, we achieve a high carrier mobility ~16,000 cm^2/Vs at room temperature with a short carrier transit time in graphene channel. On the other hand, the unique band structure of the 2D heterostructure perovskites (Fig. 20b) has built-in band bending and allows efficient electron-hole pair separation in perovskites as illustrated schematically in Fig. 20c, resulting in an enhancement of carrier lifetime ($\tau_{\_lifetime}$). As shown in Fig. 20d, we achieve a high responsivity of well above 10^3 A/W (orange dots) in a broad wavelength range of 400 to 750 nm. In comparison, the control device made from 3D perovskite shows much smaller responsivity. At the same time, the device based on 2D heterostructure perovskite shows a fast response of 14.8 ms, benefiting from the relatively shallow traps in 2D perovskites. Compared with traditional 3D perovskites integrated graphene photodetectors, our devices are superior in both responsivity and air stability. In conclusion, we demonstrated a highly sensitive photodetector based on 2D perovskites-graphene integrated structures with a high gain, high operating speed and long-term air stability. As all fabrication processes are under a low temperature < 120°C, our devices can be integrated with various substrates including flexible ones. Another major impact of this work lies in its potential in photovoltaics. The device concept and fabrication procedures developed in this project can be readily leveraged to fabricate high performance, air-stable perovskite solar cells at large scale. These results are summarized and published in Ref. [24].

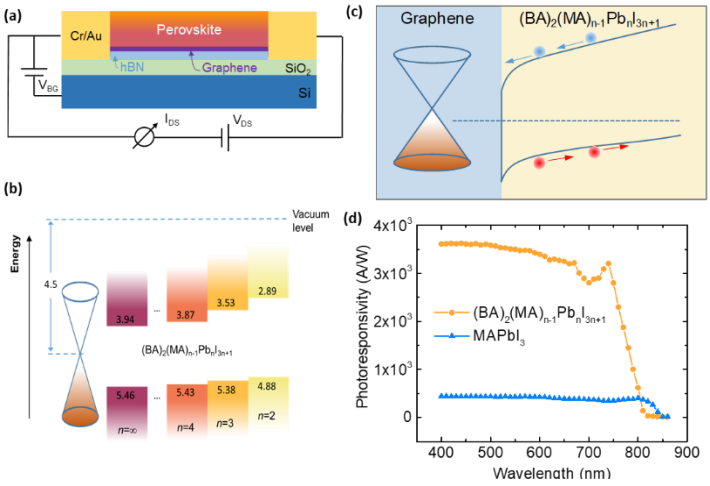

Figure 20. (**a**) The schematic image of the 2D heterostructure perovskites-graphene integrated photodetector. (**b**) The comparative band energy diagram of the $(BA)_2(MA)_{n-1}Pb_nI_{3n+1}$ perovskites with different n and graphene. (**c**) The schematic energy level diagram of the graphene-perovskite heterostructure phototransistor, illustrating a positive sloping in the energy band for photo-generated electron-hole separation. (**d**) Spectra responsivity of phototransistors with 2D perovskite heterostructure and 3D perovskite as the light absorbing material measured with V_{BG} = 15V and V_{DS} = 200 mV.

(6) *2D Topological Materials Towards Low-Energy Consumption Devices*: QSH insulator is a topologically nontrivial quantum state that features quantized Hall conductance in the absence of a magnetic field. The most pronounced characteristic electronic property of QSH state is the helical edge state protected by time reversal symmetry and the bulk band gap opening due to a strong spin-orbit coupling (SOC). The layered semimetal WTe_2 has attracted attention recently for its

extreme magnetoresistance[25] at low temperatures and its nontrivial band topology which includes type-II Weyl points[26]. In 2015 it was also predicted[27] to become a two-dimensional topological insulator, or quantum spin Hall insulator, in the monolayer limit. The **Shen** group has successfully grown monolayer 1T'-WTe_2, and observed hallmarks of QSH phase – opening of a band gap and band inversion. The collaboration with STM group directly observes the robust edge state. They also successfully synthesized monolayer 1T' phase $MoTe_2$ and WSe_2. 1T'-WSe2 is also proved to be a quantum spin hall insulator with even larger bandgap.

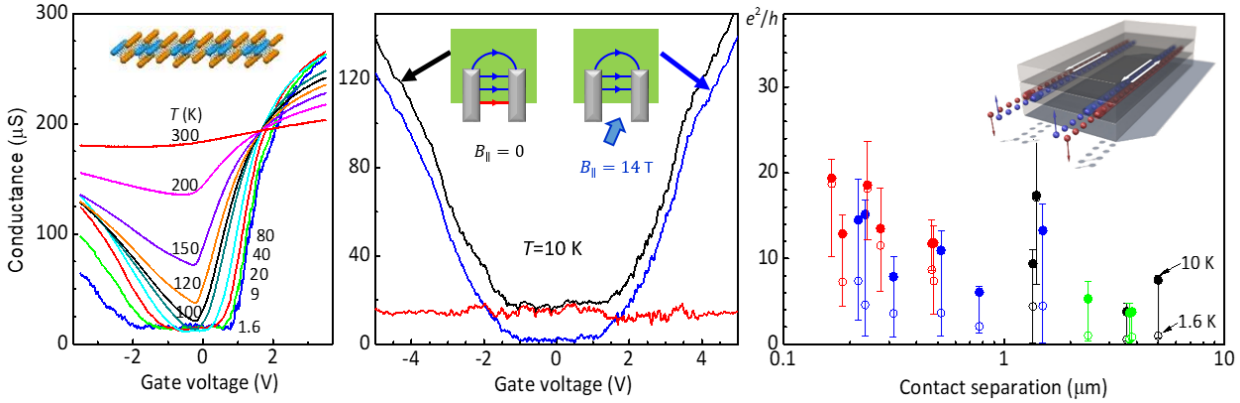

Figure 21. Left: temperature dependence of the characteristics of a monolayer WTe_2 transistor. Below 100 K a plateau due to edge conduction forms. Inset: structure of a monolayer. Middle: characteristics at 10 K with (blue) and without (black) an in-plane magnetic field, demonstrating that the edge conduction is suppressed, consistent with the edge channels being helical. Right: Length dependence of the edge conductance, approaching half the quantized value (e^2/h) for short edges. Inset: cartoon of the quantum spin Hall effect.

In parallel, **Cobden** and **Xu** prepared monolayer WTe_2 devices encapsulated in hBN to prevent oxidation, and found that on cooling below 100 K they become insulating at low gate voltages while the edges remaining conducting, consistent with the quantum spin Hall effect[28] (Fig. WTe2). The edge conduction is gapless at zero magnetic field and strongly suppressed by an in-plane field, exactly as expected for the helical edge modes (having electron spin locked to momentum) that should exist on the boundaries of a topological insulator. The conduction along a single edge between adjacent contacts also approaches about half the maximum quantum value of e^2/h =39 μS, implying that in spite of the topological protection there is significant backscattering in the helical edge which remains to be understood. Nevertheless, this is the first report of a true monolayer topological insulator, which may be combined with other 2D materials such as superconductors, semiconductors and magnets in the future to achieve spintronic and quantum information goals.

E. Complete list of publications

1. S. Tang, Z.X. Shen et al. "Electronic structure of monolayer 1T'-$MoTe_2$ grown by molecular beam epitaxy", accepted for publication, ***APL materials***.
2. S. Namgung, J. Shaver, S.-H. Oh, and S. J. Koester, "Multimodal photodiode and phototransistor device based on two-dimensional materials," ***ACS Nano*** 10, 10500–10506 (2016).

3. M. C. Robbins and S. J. Koester, "Crystal-oriented black phosphorus TFETs with strong band-to-band-tunneling anisotropy and subthreshold slope nearing the thermionic limit," ***International Electron Devices Meeting (IEDM)***, San Francisco, CA, Dec. 3-6, (2017).

4. M. R. M. Atalla and S. J. Koester, "Black phosphorus avalanche photodetector," ***75th Device Research Conference (DRC)***, Notre Dame, IN, Jun. 25-28, (2017).

5. M. C. Robbins, S. Namgung, S.-H. Oh, and S. J. Koester, "Cyclical thinning of black phosphorus with high spatial resolution for heterostructure devices," ***ACS Appl. Mater. Interfaces*** 9, 12654–12662 (2017).

6. C. Chen, N. Youngblood, R. Peng, D. Yoo, D. A. Mohr, T. W. Johnson, S.-H. Oh, and M. Li, Three-Dimensional Integration of Black Phosphorus Photodetector with Silicon Photonics and Nanoplasmonics, ***Nano Lett.*** 17, 985 (2017).

7. N. Youngblood and M. Li, Ultrafast photocurrent measurements of a black phosphorus photodetector, ***Appl. Phys. Lett.*** 110, 051102 (2017).

8. Jason Solomon Ross, Pasqual Rivera, John R. Schaibley, Eric Lee Wong, Hongyi Yu, Takashi Taniguchi, Kenji Watanabe, Jiaqiang Yan, D. Mandrus, David Henry Cobden, Wang Yao, and Xiaodong Xu, "Interlayer Exciton Optoelectronics in a 2D Heterostructure p-n Junction", ***Nano Letters*** 17, 638-643 (2017).

9. Zaiyao Fei, Tauno Palomaki, Sanfeng Wu, Wenjin Zhao, Xinghan Cai, Bosong Sun, Paul Nguyen, Joseph Finney, Xiaodong Xu, David H. Cobden, "Edge conduction in monolayer WTe2", ***Nature Physics*** doi:10.1038/nphys4091 (2017);

10. M. Xu, Y. Gu, R. Peng, N. Youngblood, and M. Li, Black phosphorus mid-infrared photodetectors, ***Appl. Phys. B*** 123, 130 (2017).

11. R. Peng, K. Khaliji, N. Youngblood, R. Grassi, T. Low, and M. Li, Midinfrared Electro-optic Modulation in Few-Layer Black Phosphorus, ***Nano Lett.*** 17, 6315 (2017).

12. S. Tang, Z.X. Shen et al. "Quantum spin Hall state in monolayer 1T'-WTe_2", ***Nat Phys*** 13, 683. (2017)

13. V. Artel, Q. Guo, H. Cohen, R. Gasper, A. Ramasubramaniam, F. Xia and D. Naveh, "Protective molecular passivation of black phosphorous," ***npj 2D Materials and Applications*** 1, 6 (2017).

14. Y. Shao, Y. Liu, X. Chen, C. Chen, I. Sarpkaya, Z. Chen, Y. Fang, J. Kong, K. Watanabe, T. Taniguchi, A. D. Taylor, J. Huang, and F. Xia, "Stable graphene-two dimensional multiphase perovskite heterostructure phototransistors with high gain," ***Nano Letters***, DOI: 10.1021/acs.nanolett.7b02980 (2017).

15. Y. Zhang, Z.X. Shen et al. "Electronic Structure, Surface Doping, and Optical Response in Epitaxial WSe_2 Thin Films", ***Nano Lett*** 16(4), 2485-2491 (2016).

16. M. Ugeda, Z.X. Shen et al. "Characterization of collective ground states in single-layer $NbSe_2$", ***Nat Phys*** 12(1), 92-97 (2016)

17. N. Sivadas, S. Okamoto, and D. Xiao, "Gate-Controllable Magneto-optic Kerr Effect in Layered Collinear Antiferromagnets", Phys. Rev. Lett. **117**, 267203 (2016).

18. John R. Schaibley, Hongyi Yu, Genevieve Clark, Pasqual Rivera, Jason S. Ross, Kyle L. Seyler, Wang Yao & Xiaodong Xu, "Valleytronics in 2D materials", ***Nature Reviews Materials*** 1, Article number: 16055 (2016).

19. S. Wu, L. Wang, Y. Lai, W.-Y. Shan, G. Aivazian, X. Zhang, T. Taniguchi, K. Watanabe, D. Xiao, C. Dean, J. Hone, Z. Li, and X. Xu, "Multiple hot-carrier collection in photo-excited graphene moire superlattices", ***Science Advance*** **2**, e1600002 (2016).

20. N. Youngblood, R. Peng, A. Nemilentsau, T. Low, and M. Li, Layer Tunable Third-Harmonic Generation in Multilayer Black Phosphorus, ACS Photonics (2016).

21. Q. Guo, A. Pospischil, M. Bhuiyan, H. Jiang, H. Tian, D. Farmer, B. Deng, C. Li, S.-J. Han, H. Wang, Q. Xia, T.-P. Ma, T. Mueller, and F. Xia, "Black Phosphorus Mid-Infrared Photodetectors with High Gain," ***Nano Letters*** 16, 4648–4655 (2016).

22. H. Tian, Q. Guo, Y. Xie, H. Zhao, C. Li, J. J. Cha, F. Xia, and H. Wang, "Anisotropic Black Phosphorus Synaptic Device for Neuromorphic Applications," ***Advanced Materials*** 28, 4991–4997 (2016).

23. Genevieve Clark, John R. Schaibley, Jason Ross, Takashi Taniguchi, Kenji Watanabe, Joshua R. Hendrickson, Shin Mou, Wang Yao, and Xiaodong Xu, "Single Defect Light-Emitting Diode in a van der Waals Heterostructure", ***Nano Letters*** DOI: 10.1021/acs.nanolett.6b01580 (2016).

24. N. Haratipour, S. Namgung, S.-H. Oh, and S. J. Koester, "Fundamental limits on the subthreshold slope in Schottky source/drain black phosphorus field-effect transistors," ***ACS Nano*** 10, 3791–3800 (2016).

25. Chang-Hua Liu, Genevieve Clark, Taylor Fryett, Sanfeng Wu, Jiajiu Zheng, Fariba Hatami, Xiaodong Xu, and Arka Majumdar, "Nanocavity Integrated van der Waals Heterostructure Light-Emitting Tunneling Diode", ***Nano Letters*** 10.1021/acs.nanolett.6b03801 (2016).

26. H. Tian, B. Deng, M. L. Chin, X. Yan, H. Jiang, S.-J. Han, V. Sun, Q. Xia, M. Dubey, F. Xia, and H. Wang, "A Dynamically Reconfigurable Ambipolar Black Phosphorus Memory Device," ***ACS Nano*** 10, 10428–10435 (2016).

27. Taylor K. Fryett, Kyle L. Seyler, Jiajiu Zheng, Chang-Hua Liu, Xiaodong Xu, Arka Majumdar, "Silicon photonic crystal cavity enhanced second-harmonic generation from monolayer WSe_2", **2D materials** 4, Number 1 (2016).

28. N. Youngblood and M. Li, Integration of 2D materials on a silicon photonics platform for optoelectronics applications, Nanophotonics (2016).

29. S. Barja, Z.X. Shen *et al.* "Charge density wave order in 1D mirror twin boundaries of single-layer $MoSe_2$", ***Nat Phys*** 2016, 12: 751.

30. W.-Y. Shan, J. Zhou, and D. Xiao, "Optical generation and detection of pure valley current in monolayer transition-metal dichalcogenides", ***Phys. Rev. B*** 91, 035402 (2015).

31. J. Zhou, W.-Y. Shan, and D. Xiao, "Spin responses and effective Hamiltonian for the two-dimensional electron gas at the oxide interface LaAlO3/SrTiO3", ***Phys. Rev. B*** 91, 241302(R) (2015)

32. J. Zhou, H.-R. Chang, and D. Xiao, “Plasmon mode as a detection of the chiral anomaly in Weyl semimetals”, ***Phys. Rev. B*** 91, 035114 (2015).

33. N. Sivadas, M. W. Daniels, R. H. Swendsen, S. Okamoto, and D. Xiao, “Magnetic ground state of semiconducting transition-metal trichalcogenide monolayers”, ***Phys. Rev. B*** 91, 235425 (2015).

34. J. Zhou, W.-Y. Shan, W. Yao, and D. Xiao, “Berry phase modification to the energy spectrum of excitons”, ***Phys. Rev. Lett.*** **115**, 166803 (2015)

35. X. Ling, H. Wang, S. Huang, F. Xia, and M. S. Dresselhaus, “The renaissance of black phosphorus,” ***Proceedings of the National Academy of Sciences*** 112, 4523-4530 (2015).

36. S. Wu, S. Buckley, J. Schaible, L. Feng, J. Yan, D. G. Mandrus, F. Hatami, W. Yao, J.Vučković, A. Majumdar, X. Xu, " Ultra-low threshold monolayer semiconductor nanocavity lasers", ***Nature*** 520, 69 (2015).

37. N. Youngblood, C. Chen, S. J. Koester, and M. Li, Waveguide-integrated black phosphorus photodetector with high responsivity and low dark current, Nat. Photon. (2015).

38. Yu-Ming He, Genevieve Clark, J. R. Schaibley, Yu He, M.-C. Chen, Y.-J. Wei1, X. Ding, Qiang Zhang, Wang Yao, Xiaodong Xu, Chao-Yang Lu, and Jian-Wei Pan, “Single Quantum Emitters in Monolayer Semiconductors”, ***Nature Nanotechnology*** 10, 497 (2015).

39. Y. Zhang, Z.X. Shen, et al. “Direct observation of the transition from indirect to direct bandgap in atomically thin epitaxial $MoSe_2$”, ***Nat Nanotech*** 2014, 9(2): 111-115.

40. F. Xia, H. Wang, D. Xiao, M. Dubey, and A. Ramasubramaniam, “Two-dimensional material and nanophotonics”, ***Nature Photonics*** 8, 899 (2014).

41. N. Youngblood, Y. Anugrah, R. Ma, S. Koester, and M. Li, Multifunctional graphene optical modulator and photodetector integrated on silicon waveguides, Nano Lett. **14**, 2741 (2014).

F. Reference

1 Xia, F., Wang, H., Xiao, D., Dubey, M. & Ramasubramaniam, A. Two-dimensional material nanophotonics. *Nature Photonics* **8**, 899.(2014).

2 Ling, X., Wang, H., Huang, S., Xia, F. & Dresselhaus, M. S. The renaissance of black phosphorus. *Proceedings of the National Academy of Sciences* **112**, 4523-4530.(2015).

3 Schaibley, J. R., Yu, H., Clark, G., Rivera, P., Ross, J. S., Seyler, K. L., Yao, W. & Xu, X. Valleytronics in 2D materials. *Nature Reviews Materials* **1**, 16055.(2016).

4 Xia, F., Wang, H. & Yang, L. Black phosphorus and its isoelectronic materials. *Manuscript in revision.* .

5 Liu, C.-H., Clark, G., Fryett, T., Wu, S., Zheng, J., Hatami, F., Xu, X. & Majumdar, A. Nanocavity Integrated van der Waals Heterostructure Light-Emitting Tunneling Diode. *Nano Letters*.(2016).

6 Wu, S., Buckley, S., Schaibley, J. R., Feng, L., Yan, J., Mandrus, D. G., Hatami, F., Yao, W., Vuckovic, J., Majumdar, A. & Xu, X. Monolayer semiconductor nanocavity lasers with ultralow thresholds. *Nature* **520**, 69-72.(2015).
7 Namgung, S., Shaver, J., Oh, S.-H. & Koester, S. J. Multimodal Photodiode and Phototransistor Device Based on Two-Dimensional Materials. *ACS Nano* **10**, 10500-10506.(2016).
8 He, Y.-M., ClarkGenevieve, SchaibleyJohn, R., He, Y., ChenMing, C., WeiYu, J., DingXing, Zhang, Q., Yao, W., Xu, X., Lu, C.-Y. & Pan, J.-W. Single quantum emitters in monolayer semiconductors. *Nat Nano* **10**, 497-502.(2015).
9 Clark, G., Schaibley, J. R., Ross, J., Taniguchi, T., Watanabe, K., Hendrickson, J. R., Mou, S., Yao, W. & Xu, X. Single Defect Light-Emitting Diode in a van der Waals Heterostructure. *Nano Letters* **16**, 3944-3948.(2016).
10 Artel, V., Guo, Q., Cohen, H., Gasper, R., Ramasubramaniam, A., Xia, F. & Naveh, D. Protective molecular passivation of black phosphorus. *npj 2D Materials and Applications* **1**, 6.(2017).
11 Youngblood, N. & Li, M. Integration of 2D materials on a silicon photonics platform for optoelectronics applications. *Nanophotonics*.(2016).
12 Youngblood, N., Anugrah, Y., Ma, R., Koester, S. & Li, M. Multifunctional graphene optical modulator and photodetector integrated on silicon waveguides. *Nano Lett.* **14**, 2741-2746.(2014).
13 Robbins, M. C., Namgung, S., Oh, S.-H. & Koester, S. J. Cyclical Thinning of Black Phosphorus with High Spatial Resolution for Heterostructure Devices. *ACS Applied Materials & Interfaces* **9**, 12654-12662.(2017).
14 Haratipour, N., Namgung, S., Oh, S.-H. & Koester, S. J. Fundamental Limits on the Subthreshold Slope in Schottky Source/Drain Black Phosphorus Field-Effect Transistors. *ACS Nano* **10**, 3791-3800.(2016).
15 Robbins, M. C. & Koester, S. J. Crystal-oriented black phosphorus TFETs with strong band-to-band-tunneling anisotropy and subthreshold slope nearing the thermionic limit. *International Electron Devices Meeting (IEDM), San Francisco, CA, Dec. 3-6, 2017.*
16 Xu, M., Gu, Y., Peng, R., Youngblood, N. & Li, M. Black phosphorus mid-infrared photodetectors. *Appl. Phys. B* **123**, 130.(2017).
17 Guo, Q., Pospischil, A., Bhuiyan, M., Jiang, H., Tian, H., Farmer, D., Deng, B., Li, C., Han, S.-J., Wang, H., Xia, Q., Ma, T.-P., Mueller, T. & Xia, F. Black Phosphorus Mid-Infrared Photodetectors with High Gain. *Nano Letters* **16**, 4648-4655.(2016).
18 Peng, R., Khaliji, K., Youngblood, N., Grassi, R., Low, T. & Li, M. Midinfrared Electro-optic Modulation in Few-Layer Black Phosphorus. *Nano Lett.* **17**, 6315-6320.(2017).
19 Yuan, S., Shen, C., Deng, B., Chen, X., Guo, Q., Ma, Y., Abbass, A., Liu, B., Haiges, R., Ott, C., Nilges, T., Watanabe, K., Taniguchi, T., Sinai, O., Naveh, D., Zhou, C. & Xia, F. Air-stable room-temperature mid-infrared photodetectors based on hBN/black arsenic phosphorus/hBN heterostructures. *Manuscript in submission.* .
20 Youngblood, N. & Li, M. Ultrafast photocurrent measurements of a black phosphorus photodetector. *Appl. Phys. Lett.* **110**, 051102.(2017).
21 Youngblood, N., Chen, C., Koester, S. J. & Li, M. Waveguide-integrated black phosphorus photodetector with high responsivity and low dark current. *Nat. Photon.*(2015).

22 Chen, C., Youngblood, N., Peng, R., Yoo, D., Mohr, D. A., Johnson, T. W., Oh, S.-H. & Li, M. Three-Dimensional Integration of Black Phosphorus Photodetector with Silicon Photonics and Nanoplasmonics. *Nano Lett.* **17**, 985-991.(2017).
23 Youngblood, N., Peng, R., Nemilentsau, A., Low, T. & Li, M. Layer Tunable Third-Harmonic Generation in Multilayer Black Phosphorus. *ACS Photonics*.(2016).
24 Shao, Y., Liu, Y., Chen, X., Chen, C., Sarpkaya, i., Chen, Z., Fang, Y., Kong, J., Watanabe, K., Taniguchi, T., Taylor, A. D., Huang, J. & Xia, F. Stable graphene-two dimensional multiphase perovskite heterostructure phototransistors with high gain. *Nano Letters*.(2017).
25 Ali, M. N., Xiong, J., Flynn, S., Tao, J., Gibson, Q. D., Schoop, L. M., Liang, T., Haldolaarachchige, N., Hirschberger, M., Ong, N. P. & Cava, R. J. Large, non-saturating magnetoresistance in WTe_2. *Nature* **514**, 205-208.(2014).
26 Soluyanov, A. A., Gresch, D., Wang, Z., Wu, Q., Troyer, M., Dai, X. & Bernevig, B. A. Type-II Weyl semimetals. *Nature* **527**, 495-498.(2015).
27 Qian, X., Liu, J., Fu, L. & Li, J. Quantum spin Hall effect in two-dimensional transition metal dichalcogenides. *Science* **346**, 1344-1347.(2014).
28 Fei, Z., Palomaki, T., Wu, S., Zhao, W., Cai, X., Sun, B., Nguyen, P., Finney, J., Xu, X. & Cobden, D. H. Edge conduction in monolayer WTe_2. *Nat Phys* **13**, 677-682.(2017).

AFOSR Deliverables Submission Survey

Response ID:9036 Data

1.

Report Type

Final Report

Primary Contact Email

Contact email if there is a problem with the report.

xuxd@uw.edu

Primary Contact Phone Number

Contact phone number if there is a problem with the report

2065438444

Organization / Institution name

U Washington

Grant/Contract Title

The full title of the funded effort.

2D Heterostructures for Integrated Nano-Optoelectronics

Grant/Contract Number

AFOSR assigned control number. It must begin with "FA9550" or "F49620" or "FA2386".

FA9550-14-1-0277

Principal Investigator Name

The full name of the principal investigator on the grant or contract.

Xiaodong Xu

Program Officer

The AFOSR Program Officer currently assigned to the award

Gernot Pomrenke

Reporting Period Start Date

09/15/2014

Reporting Period End Date

09/14/2017

Abstract

The BRI project aims to investigate the use of novel nano-optoelectronic systems based upon two-dimensional (2D) heterostructures to realize breakthrough technologies for optical communications. The 2D heterostructure devices feature atomically-thin transition metal dichalcogenides (TMDs) and black phosphorous, in combination with graphene and boron nitride. During this award period, we have made exciting progress towards the objective, including material innovation, device engineering, and development and investigation of 2D optoelectronics and integration with nano-photonic structures. In specific: (1) We have developed layer by layer growth of a wide range of TMDs by both MBE and physical vapor transport. (2) We have developed both TMD based optoelectronic devices near visible wavelength range and black-phosphorus based mid-infrared optoelectronics. These devices include light emitting diodes (LEDs), nano-cavity integrated monolayer LEDs, 2D heterostructure LEDs, optical and electrical driven single quantum emitters in monolayer WSe2, and mid-Infrared black phosphorus photodetector with electrical control; (4) development of novel materials and device concepts, such as the discovery of 2D topological insulators for low energy dissipation devices. The success of our program will lead to disruptive optical technologies for long and short-distance communication, with low power, high density, and high

bandwidth for both civilian and military needs.

Distribution Statement

This is block 12 on the SF298 form.

Distribution A - Approved for Public Release

Explanation for Distribution Statement

If this is not approved for public release, please provide a short explanation. E.g., contains proprietary information.

SF298 Form

Please attach your SF298 form. A blank SF298 can be found here. Please do not password protect or secure the PDF The maximum file size for an SF298 is 50MB.

SF_298_11-22-2017_v2.pdf

Upload the Report Document. File must be a PDF. Please do not password protect or secure the PDF . The maximum file size for the Report Document is 50MB.

Final-Report-FA9550-14-1-0277.pdf

Upload a Report Document, if any. The maximum file size for the Report Document is 50MB.

Archival Publications (published) during reporting period:

1. S. Tang, Z.X. Shen et al. "Electronic structure of monolayer 1T'-MoTe2 grown by molecular beam epitaxy", accepted for publication, APL materials.
2. S. Namgung, J. Shaver, S.-H. Oh, and S. J. Koester, "Multimodal photodiode and phototransistor device based on two-dimensional materials," ACS Nano 10, 10500–10506 (2016).
3. M. C. Robbins and S. J. Koester, "Crystal-oriented black phosphorus TFETs with strong band-to-band-tunneling anisotropy and subthreshold slope nearing the thermionic limit," International Electron Devices Meeting (IEDM), San Francisco, CA, Dec. 3-6, (2017).
4. M. R. M. Atalla and S. J. Koester, "Black phosphorus avalanche photodetector," 75th Device Research Conference (DRC), Notre Dame, IN, Jun. 25-28, (2017).
5. M. C. Robbins, S. Namgung, S.-H. Oh, and S. J. Koester, "Cyclical thinning of black phosphorus with high spatial resolution for heterostructure devices," ACS Appl. Mater. Interfaces 9, 12654–12662 (2017).
6. C. Chen, N. Youngblood, R. Peng, D. Yoo, D. A. Mohr, T. W. Johnson, S.-H. Oh, and M. Li, Three-Dimensional Integration of Black Phosphorus Photodetector with Silicon Photonics and Nanoplasmonics, Nano Lett. 17, 985 (2017).
7. N. Youngblood and M. Li, Ultrafast photocurrent measurements of a black phosphorus photodetector, Appl. Phys. Lett. 110, 051102 (2017).
8. Jason Solomon Ross, Pasqual Rivera, John R. Schaibley, Eric Lee Wong, Hongyi Yu, Takashi Taniguchi, Kenji Watanabe, Jiaqiang Yan, D. Mandrus, David Henry Cobden, Wang Yao, and Xiaodong Xu, "Interlayer Exciton Optoelectronics in a 2D Heterostructure p-n Junction", Nano Letters 17, 638-643 (2017).
9. Zaiyao Fei, Tauno Palomaki, Sanfeng Wu, Wenjin Zhao, Xinghan Cai, Bosong Sun, Paul Nguyen, Joseph Finney, Xiaodong Xu, David H. Cobden, "Edge conduction in monolayer WTe2", Nature Physics doi:10.1038/nphys4091 (2017);
10. M. Xu, Y. Gu, R. Peng, N. Youngblood, and M. Li, Black phosphorus mid-infrared photodetectors, Appl. Phys. B 123, 130 (2017).
11. R. Peng, K. Khaliji, N. Youngblood, R. Grassi, T. Low, and M. Li, Midinfrared Electro-optic Modulation in Few-Layer Black Phosphorus, Nano Lett. 17, 6315 (2017).
12. S. Tang, Z.X. Shen et al. "Quantum spin Hall state in monolayer 1T'-WTe2", Nat Phys 13, 683. (2017)
13. V. Artel, Q. Guo, H. Cohen, R. Gasper, A. Ramasubramaniam, F. Xia and D. Naveh, "Protective molecular passivation of black phosphorous," npj 2D Materials and Applications 1, 6 (2017).
14. Y. Shao, Y. Liu, X. Chen, C. Chen, I. Sarpkaya, Z. Chen, Y. Fang, J. Kong, K. Watanabe, T. Taniguchi, A. D. Taylor, J. Huang, and F. Xia, "Stable graphene-two dimensional multiphase perovskite heterostructure phototransistors with high gain," Nano Letters, DOI: 10.1021/acs.nanolett.7b02980 (2017).
15. Y. Zhang, Z.X. Shen et al. "Electronic Structure, Surface Doping, and Optical Response in Epitaxial WSe2 Thin Films", Nano Lett 16(4), 2485-2491 (2016).

16. M. Ugeda, Z.X. Shen et al. "Characterization of collective ground states in single-layer NbSe2", Nat Phys 12(1), 92-97 (2016)
17. N. Sivadas, S. Okamoto, and D. Xiao, "Gate-Controllable Magneto-optic Kerr Effect in Layered Collinear Antiferromagnets", Phys. Rev. Lett. 117, 267203 (2016).
18. John R. Schaibley, Hongyi Yu, Genevieve Clark, Pasqual Rivera, Jason S. Ross, Kyle L. Seyler, Wang Yao & Xiaodong Xu, "Valleytronics in 2D materials", Nature Reviews Materials 1, Article number: 16055 (2016).
19. S. Wu, L. Wang, Y. Lai, W.-Y. Shan, G. Aivazian, X. Zhang, T. Taniguchi, K. Watanabe, D. Xiao, C. Dean, J. Hone, Z. Li, and X. Xu, "Multiple hot-carrier collection in photo-excited graphene moire superlattices", Science Advance 2, e1600002 (2016).
20. N. Youngblood, R. Peng, A. Nemilentsau, T. Low, and M. Li, Layer Tunable Third-Harmonic Generation in Multilayer Black Phosphorus, ACS Photonics (2016).
21. Q. Guo, A. Pospischil, M. Bhuiyan, H. Jiang, H. Tian, D. Farmer, B. Deng, C. Li, S.-J. Han, H. Wang, Q. Xia, T.-P. Ma, T. Mueller, and F. Xia, "Black Phosphorus Mid-Infrared Photodetectors with High Gain," Nano Letters 16, 4648–4655 (2016).
22. H. Tian, Q. Guo, Y. Xie, H. Zhao, C. Li, J. J. Cha, F. Xia, and H. Wang, "Anisotropic Black Phosphorus Synaptic Device for Neuromorphic Applications," Advanced Materials 28, 4991–4997 (2016).
23. Genevieve Clark, John R. Schaibley, Jason Ross, Takashi Taniguchi, Kenji Watanabe, Joshua R. Hendrickson, Shin Mou, Wang Yao, and Xiaodong Xu, "Single Defect Light-Emitting Diode in a van der Waals Heterostructure", Nano Letters DOI: 10.1021/acs.nanolett.6b01580 (2016).
24. N. Haratipour, S. Namgung, S.-H. Oh, and S. J. Koester, "Fundamental limits on the subthreshold slope in Schottky source/drain black phosphorus field-effect transistors," ACS Nano 10, 3791–3800 (2016).
25. Chang-Hua Liu, Genevieve Clark, Taylor Fryett, Sanfeng Wu, Jiajiu Zheng, Fariba Hatami, Xiaodong Xu, and Arka Majumdar, "Nanocavity Integrated van der Waals Heterostructure Light-Emitting Tunneling Diode", Nano Letters 10.1021/acs.nanolett.6b03801 (2016).
26. H. Tian, B. Deng, M. L. Chin, X. Yan, H. Jiang, S.-J. Han, V. Sun, Q. Xia, M. Dubey, F. Xia, and H. Wang, "A Dynamically Reconfigurable Ambipolar Black Phosphorus Memory Device," ACS Nano 10, 10428–10435 (2016).
27. Taylor K. Fryett, Kyle L. Seyler, Jiajiu Zheng, Chang-Hua Liu, Xiaodong Xu, Arka Majumdar, "Silicon photonic crystal cavity enhanced second-harmonic generation from monolayer WSe2", 2D materials 4, Number 1 (2016).
28. N. Youngblood and M. Li, Integration of 2D materials on a silicon photonics platform for optoelectronics applications, Nanophotonics (2016).
29. S. Barja, Z.X. Shen et al. "Charge density wave order in 1D mirror twin boundaries of single-layer MoSe2", Nat Phys 2016, 12: 751.
30. W.-Y. Shan, J. Zhou, and D. Xiao, "Optical generation and detection of pure valley current in monolayer transition-metal dichalcogenides", Phys. Rev. B 91, 035402 (2015).
31. J. Zhou, W.-Y. Shan, and D. Xiao, "Spin responses and effective Hamiltonian for the two-dimensional electron gas at the oxide interface LaAlO3/SrTiO3", Phys. Rev. B 91, 241302(R) (2015)
32. J. Zhou, H.-R. Chang, and D. Xiao, "Plasmon mode as a detection of the chiral anomaly in Weyl semimetals", Phys. Rev. B 91, 035114 (2015).
33. N. Sivadas, M. W. Daniels, R. H. Swendsen, S. Okamoto, and D. Xiao, "Magnetic ground state of semiconducting transition-metal trichalcogenide monolayers", Phys. Rev. B 91, 235425 (2015).
34. J. Zhou, W.-Y. Shan, W. Yao, and D. Xiao, "Berry phase modification to the energy spectrum of excitons", Phys. Rev. Lett. 115, 166803 (2015)
35. X. Ling, H. Wang, S. Huang, F. Xia, and M. S. Dresselhaus, "The renaissance of black phosphorus," Proceedings of the National Academy of Sciences 112, 4523-4530 (2015).
36. S. Wu, S. Buckley, J. Schaible, L. Feng, J. Yan, D. G. Mandrus, F. Hatami, W. Yao, J.Vučković, A. Majumdar, X. Xu, " Ultra-low threshold monolayer semiconductor nanocavity lasers", Nature 520, 69 (2015).
37. N. Youngblood, C. Chen, S. J. Koester, and M. Li, Waveguide-integrated black phosphorus photodetector with high responsivity and low dark current, Nat. Photon. (2015).
38. Yu-Ming He, Genevieve Clark, J. R. Schaibley, Yu He, M.-C. Chen, Y.-J. Wei1, X. Ding, Qiang Zhang,

Wang Yao, Xiaodong Xu, Chao-Yang Lu, and Jian-Wei Pan, "Single Quantum Emitters in Monolayer Semiconductors", Nature Nanotechnology 10, 497 (2015).
39. Y. Zhang, Z.X. Shen, et al. "Direct observation of the transition from indirect to direct bandgap in atomically thin epitaxial MoSe2", Nat Nanotech 2014, 9(2): 111-115.
40. F. Xia, H. Wang, D. Xiao, M. Dubey, and A. Ramasubramaniam, "Two-dimensional material and nanophotonics", Nature Photonics 8, 899 (2014).
41. N. Youngblood, Y. Anugrah, R. Ma, S. Koester, and M. Li, Multifunctional graphene optical modulator and photodetector integrated on silicon waveguides, Nano Lett. 14, 2741 (2014).

New discoveries, inventions, or patent disclosures:

Do you have any discoveries, inventions, or patent disclosures to report for this period?

No

Please describe and include any notable dates

Do you plan to pursue a claim for personal or organizational intellectual property?

Changes in research objectives (if any):

N/A

Change in AFOSR Program Officer, if any:

N/A

Extensions granted or milestones slipped, if any:

N/A

AFOSR LRIR Number

LRIR Title

Reporting Period

Laboratory Task Manager

Program Officer

Research Objectives

Technical Summary

Funding Summary by Cost Category (by FY, $K)

	Starting FY	FY+1	FY+2
Salary			
Equipment/Facilities			
Supplies			
Total			

Report Document

Report Document - Text Analysis

Report Document - Text Analysis

Appendix Documents

2. Thank You

E-mail user

Nov 28, 2017 18:49:55 Success: Email Sent to: xuxd@uw.edu